Project of an UAV of infinite autonomy

REPORT

AUTHOR
Sánchez Bravo, Àlex

DIRECTOR
Pérez Llera, Luis Manuel

ESEIAAT
Polytechnic University of Catalonia

Delivery date
10/06/2019

Contents

List of Tables **iii**

List of Figures **iv**

Abstract **v**

1 Introduction **1**

1.1 Aim . . . 1

1.2 Requirements . . . 1

1.3 Scope . . . 1

1.4 Calendar . . . 2

1.5 Background . . . 5

1.5.1 The idea behind HALE UAV . . . 5

1.5.2 State of the art . . . 5

1.5.3 Environmental Impact . . . 7

2 Onboard Systems **8**

2.1 Flight Control System . . . 8

2.2 Power Supply . . . 9

3 Environmental Conditions **12**

3.1 Introducing the Stratosphere . . . 12

3.2 Radiation Incidence . . . 13

3.3 Cloud Height . . . 13

3.4 Air properties . . . 15

4 Conceptual Design **16**

4.1 Aerodynamics . . . 16

4.2 Power estimation . . . 20

4.3 Weight estimation . . . 20

4.4 Radiation Approach . . . 21

4.5 Methodology . . . 23

4.6 Results . . . 24

4.7 Tail sizing 26
4.8 Aerodynamic validation 27

5 Aerodynamics **29**
5.1 Stability Criterion 29
5.2 Typical tail vs T tail 29
5.3 Final Configuration 30

6 Structure **32**
6.1 Layout of the structure 32
6.2 Airframe 33
6.2.1 Ribs 33
6.2.2 Skin 34
6.2.3 Spars 34
6.3 Non-structural Weight 34
6.3.1 Batteries 35
6.3.2 Solar Cells 35
6.4 Weight Refinement Methodology 36
6.5 Center of Gravity 37
6.6 Structural Validation 38

7 Propulsion **40**
7.1 Propeller 40
7.2 Motor 41
7.3 Gearbox 41

8 Conclusions **42**
8.1 Further Work 43
8.2 A Comment of the Author 44

References **45**

List of Tables

1 Specifications of the HELIOS HP01 prototype. From Wikipedia [b] webpage. 6
2 Specifications of the Airbus Zephyr 7. From Wikipedia [c]. 6
3 VECTOR's main features (from UAVN webpage). 8
4 TELEM05's main features (from UAVN webpage). 9
5 Specs of the driver motor DA 15-N-ISS. Obtained from [VOLZ] webpage. 9
6 Characteristics of triple junction solar cells and solar sheets (from MicroLink webpage). 10
7 Characteristics of one 20Ah Licerion ® Cell. 10
8 Aircraft characteristics at the Conceptual Design stage. 26
9 Physical Characteristics of the plane; Conceptual Design configuration. 27
10 Main aerodynamic parameters of the final configuration. 30
11 Relevant physical characteristics of the ROHACELL HERO. 33
12 Relevant properties of HOSTAPHAN® film. 34
13 Physical properties of M60JB Toray's CFRP. 35
14 Breakdown of the c.g. calculation of the UAV 37
15 Airframe mass breakdown. 37
16 Breakdown of the c.g. calculation of the Airframe. 37
17 Main dimensions and characteristics of the propeller design. Obtained with [JavaProp]. 40
18 Specs of Xoar Propeller model PJP-T-L 40x10. Obtained from [Xoar] webpage. 40
19 Specifications of the Maxon RE motor (serial number 148867). From [Maxon] webpage. 41
20 Specifications of the Faulhaber gearbox of the Series 17/1. Obtained from [Faulhaber] webpage. 41

List of Figures

1 Other relevant specs of Licerion® 20Ah cells. 11

2 Average Incidence Radiation on June (0^{o} latitude, 25^{o} longitude) 14

3 1-year averaged measurement of frequency of ocurrence of cirrus clouds. Extracted from [Sassen et al., 2008]. 14

4 Latitudinal distribution of cirrus cloud heights. The black line shows the averaged tropopause height. Data averaged over 1 year. Extracted from Sassen et al. [2008]. . 15

5 Polar and lift plot of the E214. Extracted from: Airfoils at low speeds, 1989. 17

6 Polar and lift plot of the RG15. Extracted from: Airfoils at low speeds, 1989. 18

7 Polar and lift plot of the SD7003. Extracted from: Airfoils at low speeds, 1989. 18

8 Polar and lift plot of the SD7037. Extracted from: Airfoils at low speeds, 1989. 19

9 Energy per unit surface associated to each time step. Each hour has been divided in 5. 22

10 Point where the batteries switch giving/receiving energy. Time is in seconds and energy in Joules. 23

11 Evolution of the weights of the aircraft as a function of Sw and AR 25

12 Screenshot of the XFLR5 representation of Configuration 1. Viscous drag is represented in purple and induced drag in yellow. 28

13 Aerodynamic plots for Configuration 1. Obtained with XFLR5, ring vortex VLM with tilted geometry. 28

14 Viscous (purple) and induced (yellow) drag for two different tail configurations 30

15 CAD representation of the structure of the UAV. 32

16 Structural Analysis along the semispar of the wing; 49,05N applied at the tip. 38

17 Mesh employed in the structural analysis of the semispar. 39

Abstract

The purpose of this project has been the design an Unmanned Aerial Vehicle (UAV) able to fly virtually forever. During day hours such UAV gathers energy from solar panels placed on its wings: one part of this energy is used to keep a levelled flight (i.e. for propulsion and to keep all the other systems alive) and another part of the energy is stored in the batteries. At nightfall the UAV should have collected enough energy in the batteries to be able to operate all night. This way the designed aircraft is able to keep a levelled, energy balanced flight continuously for 24 hours, closing the cycle and being able to repeat this process again. Apart from the energy balance, the UAV has two other restrictions: it must be able to communicate with ground (i.e. to receive instructions and send data) and it includes a Global Positioning System (GPS) aboard.

However, truly infinite autonomy is impossible to reach; there will be factors that will degrade the performance of the aircraft (solar cells malfunction, moisture absortion, single or multiple element failure, etc.) and won't allow the UAV to fly forever. For this reason we will call *Infinite autonomy* the act of closing the loop: that is, to have the batteries replenished every nightfall without any loss of altitude regarding the day before. It should be noted that this has already been reached by some aircraft, with more or less success, something that will be commented briefly. More than a novel investigation, then, this work is a glance at leading technology and new technological possibilities through the preliminary design of an actual solar powered HALE UAV. In the end, a personal assessment of the possibilities and difficulties of this type of aircraft will be done.

The most outstanding challenge of this project, what makes this design more remarkably different from that of typical aircraft is the lack of previous similar planes. The usual habit, when nothing is set other than the requirements of the aircraft, is to rely on data from similar planes in the first step of the designing path —the Conceptual Design. The main difficulty of this project has just been the calculation of the weight of the aircraft, which is calculated this way: the very low wing loading and that the structure and materials had little in common with those of usual planes.

The methodology of this thesis, in broad terms, has been structured as follows: first an initial study was conducted to gain knowledge on previous similar airplanes, the altitude of operation was also studied and chosen, and the onboard systems that the aircraft would carry were detailed. The initial conditions being defined, a conceptual design was made using approximations from the literature, with the complication that not always estimations for this kind of aircraft were found — this stage defined the main wing of the aircraft in a way that the energy balance was reached and the weight of the payload was maximum. The third and last stage of the design was the preliminary design of the aircraft, in which the design went one step further in complexity: the power plant and the aerodynamic and structural configurations of the plane were defined in a concurrent way. The final configuration of the plane yielded a $9,975m^2$ wing surface, $13m/s$ cruise velocity and $9,2kg$ of weight, with capability of carrying an additional 800 grams (of payload or to account for unexpected variations in the weight).
The initial study can be found in this document from sections 1 to 3, the conceptual design is all explained in section 4 and the preliminary design occupies sections 5 to 7. Then section 8 concludes the work with an overview of the work done and the future steps to follow if the design of this plane is continued.

It should also be mentioned that no budget restrictions have been imposed. Of all the assumptions made in this document, this may well be the most unreal one. However, the aim of this thesis is none other than studying the feasibility of the infinite autonomy of an UAV. In the knowledge that this type of aircraft is mainly unstudied, it is expected to be expensive and we should not let this, in the first place, upset the desire of the *Infinite Flight*.

1 Introduction

1.1 Aim

The purpose of this project is to design an Unmanned Aerial Vehicle (UAV) able to fly virtually forever. Hence, it would recharge the batteries with solar cells during the day and use the power of the batteries to keep flying during the night.

1.2 Requirements

The UAV should be able to fly virtually forever. Apart from the essential components to make the flight possible, it should carry a Global Positioning System (GPS) and a communications system in order to be capable to receive and send information from ground.

1.3 Scope

The initial objectives of the project and the scope of each of them are detailed next:

- The solar panels and the batteries will be designed so that there is enough power available for the traction motors at any time during day and night.
- The sensors to measure position and attitude will be chosen, as well as a controller to make the necessary corrections and the motors that will drive the control surfaces.
- Optimum propeller/s will be designed for the specific flight conditions required. The main motor/s propelling the aircraft will be chosen.
- Other components of the electric system will be chosen if required.
- An communications system will be chosen in order to communicate with ground.
- The basic aerodynamic surfaces will be designed so that they are optimum for the flight conditions. This includes the wing and the tail stabilizers, as well as the design of the control surfaces that provide attitude control to the aircraft.
- The fuselage will be sized in order to fit all the components of the aircraft. However, it won't be optimized in the aerodynamic aspect.
- The cost of both the design and the aircraft itself will be estimated.
- A basic structural analysis will be made in order to ensure the integrity of the aircraft.
- The static stability of the aircraft will be studied to ensure control of the aircraft at any given moment.
- A 3D design of the aircraft, along with the pertinent drawings, will be made in order to visualize the results.

1.4 Calendar

List of tasks

Once the scope of the project has been described, the following step is to define the specific tasks that have to be carried out in order to reach the aim of the project. They are listed below:

- AERODYNAMICS (A)
  1. Selection of a profile: choose one taking into account the low Reynolds and looking at similar aircraft (gliders).
  2. Estimate the basic parameters of the wing (Cl, Cd, Cm) considering a high aspect ratio and low number of Reynolds.
  3. Approximate the required thrust.
  4. Define the external geometry of the wing.
  5. Dimensioning of the basic tail surfaces.
  6. Preliminary dimensioning of the contol surfaces.
  7. Calculate the final aerodynamic parameters of the aircraft.
  8. Study of longitudinal stability and choice of the distance of the tail.
  9. Study of lateral stability.
  10. Choose the optimum space to operate the aircraft
- SYSTEMS (SY)
  1. Look for a GPS.
  2. Look for a communications system.
  3. Look for a control system.
  4. Look for the motors driving the control surfaces.
  5. Look for optimum batteries for the aircraft.
  6. Look for optimum solar cells.
  7. Design a propeller to fit the needs of the aircraft (with the blade element theory).
  8. Look for an optimum propelling motor.
  9. Look for any additional systems needed.
- STRUCTURE (ST)
  1. Conceptual design of the aircraft based on the basic parameters.
  2. Estimation of the weight of the structure as a function of the wing span.
  3. Computation of the loads of the aircraft during cruise.
- BUDGET (B)
  1. Estimate the cost of the aircraft gathering the cost of the individual pieces.
  2. Estimate the cost of the design.
- OTHERS (O)
  1. Define the format of the project report.
  2. Revise the report and make the final modifications.

Gantt chart

Besides the characterisation of the tasks, another important step is to define a calendar for the project, which has been done in the shape of a Gantt chart. The average amount of time dedicated per week will be of 23 hours. Of those 23 hours, eleven will be during the week and the other twelve hours will be condensed on the weekend. With this weekly plan, the distribution of the tasks is set as follows:

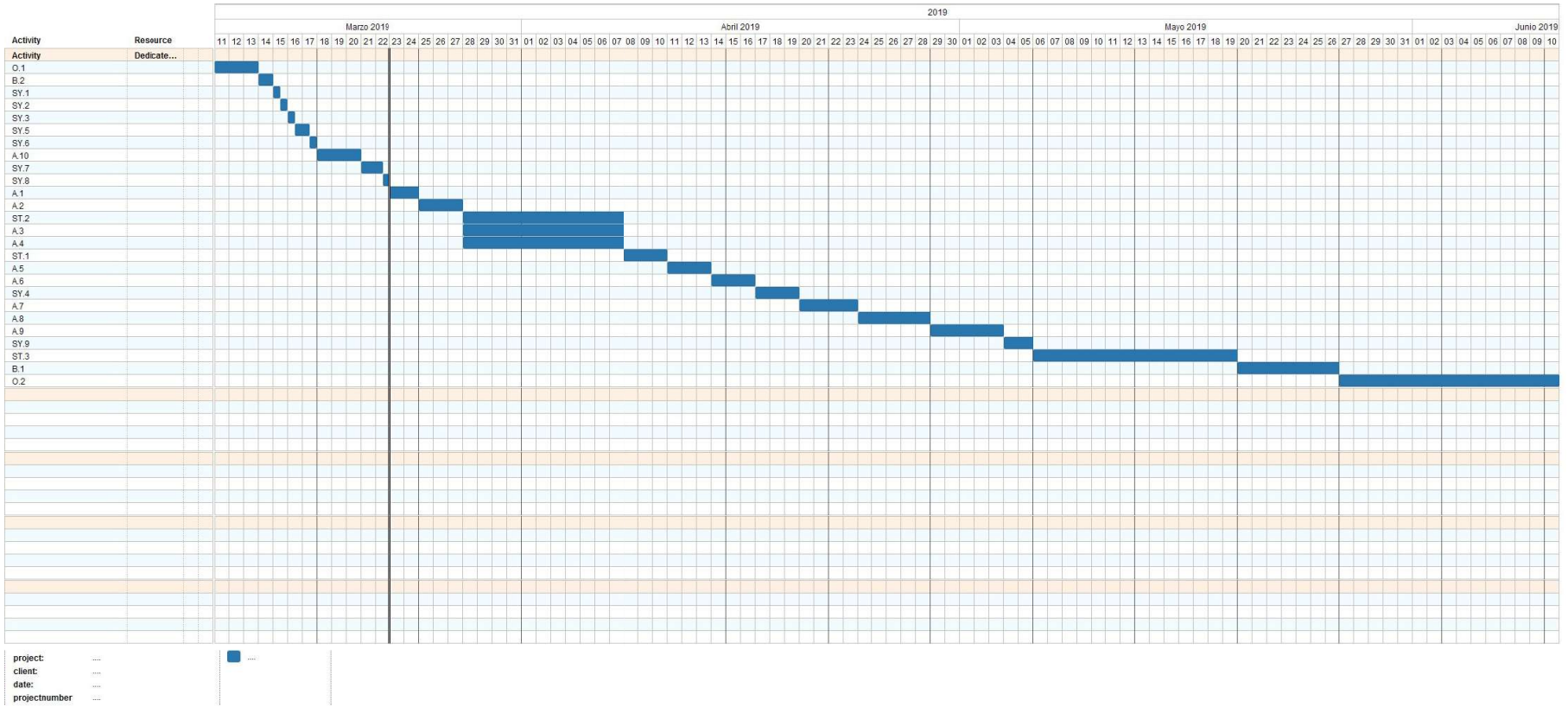
2019
Marzo 2019
Abril 2019
Mayo 2019
Junio 2019
Activity
Resource
Activity
Dedicate...
O.1
B.2
SY.1
SY.2
SY.3
SY.5
SY.6
A.10
SY.7
SY.8
A.1
A.2
ST.2
A.3
A.4
ST.1
A.5
A.6
SY.4
A.7
A.8
A.9
SY.9
ST.3
B.1
O.2
project:
client:
date:
projectnumber

1.5 Background

1.5.1 The idea behind HALE UAV

One of the first decisions to be made regarding the aircraft was to choose a location for it to fly. The equator seemed a good place because of the high irradiance it receives from the sun. But what had to be the cruise altitude of the plane? In order to fly virtually forever, the plane should fly above the clouds. Otherwise, a cloudy day could easily make the aircraft compelled to land (or cause a crash). The UAV of this thesis will be flying in the stratosphere, just beyond the tropopause. Therefore, our aicraft will be a solar powered HALE (High Altitude Long Endurance) UAV.

Because they move slowly and can keep flying for long periods of time, HALE aircraft are specially well suited for communications, where they offer different features than satellites, and for weather monitoring (apart from military purposes). And because they are located at a specific zone for long periods of time they can provide stable communication links or continuous surveillance, something satellites are unable to do.

Regarding their structure, HALE UAV tend to have different characteristcs than typical aircraft. A good example of this can be found in the patent of the Centurion aircraft, the predecessor of the HELIOS aircraft. The summarized idea behind the aircraft is as follows [Hibbs et al., 1998]: "[...] the present aircraft is unlike many conventional aircraft structures, which use a heavy main wing spar to transfer a large amount of lift to help support a fuselage and tail structure during flight. Rather, each section of the preferred aircraft has its own airfoil and, therefore, there is no significant portion of the aircraft that does not produce its own lift. Thus, the present aircraft does not need to compensate for non-lifting structures, such as a fuselage, and does not require a strong spar to stay airborne". This extract exemplifies the different nature of solar powered HALE UAV over typical commercial aircraft, and also over sailplanes. Although their design not always follows the same path, the idea of low wing loading and distributed loads along the wingspan is shared by most of them and is obviously a good strategy to follow.

1.5.2 State of the art

Now it is time to talk about previous similar aircraft. In our case, this means focusing on HALE UAV, specifically on Solar Powered HALE UAV. The study of similar existing aircraft is very important, as it allows for the estimation of some parameters before even defining the shape of the plane. To mention two, the range of Reynolds and the weight of the airframe can be estimated from similar aircraft, always taking care that the projects are alike and the same design paths apply.

The main projects in the category of Solar Powered HALE UAV are: the HELIOS prototype under NASA's Environmental Research Aircraft and Sensor Technology (ERAST) programme; the Zephyr series of aircraft, currently part of the High Altitude Pseudo-Satellite (HAPS) programme of Airbus; the Pegasus UAV; the HELIPLAT (HELIos PLATform), an ESA programme; the LA-252, designed by Russia's Lavochkin design bureau. Among those, we'll see now the characteristics of the HELIOS and the Airbus Zephyr 7, which will be useful later. For the other aircraft mentioned either the information is scarce or they haven't been tested yet, so their success is still doubtful.

HELIOS

The HELIOS prototype was developed by AeroVironment, Inc. under NASA's ERAST programme. It was the last out of four prototypes developed in this programme and was aimed to prepare the technology that would allow HALE UAV to be used as atmospheric satellites, for surveillance and communications purposes. The HELIOS prototype was a flying wing and had a modular design which promoted that every section of the wing was capable to sustain its own weight. This allowed the main spar to be lighter (and weaker), as it did not have to withstand an important bending moment anywhere along the wingspan.

The HELIOS prototype was able to reach an altitude of more than 29.000 meters, which supposed a world record of altitude at the time. There were two versions of this aricraft: the HP01, powered with batteries and solar cells; and the HP03, which used a combination of solar cells, electric batteries and an hydrogen fuel cell system to power the aircraft at night. Next are exposed the main characteristics of the HELIOS HP01, for the system it uses to reach energy balance is more similar to our design (table 1).

Chord	2,4 m
Wingspan	75,3 m
Aspect Ratio	30,9
Airspeed	8,5 - 12,1 m/s
Empty Weight	600 kg
Engine Power	21 kW (1,5 kW each)

Table 1: Specifications of the HELIOS HP01 prototype. From Wikipedia [b] webpage.

Zephyr

Zephyr is a family of solar powered UAV originally developed by QinetiQ and now part of the HAPS programme of the Airbus Group. The Zephyr's structure is made mainly of carbon fiber and was designed for observation and communications purposes, just as the HELIOS prototype. Its batteries are provided by the manufacturer Sion, one of the leaders of the sector. One of the models of the family, the Zephyr S, currently holds the world record of endurance for an UAV (almost 26 days of unrefuelled flight). Unlike NASA's prototypes, the Zephyr family has no landing gears; they are lauched by hand by some members of the crew and it will land on its belly afterwards [Desmond and Boscarol, 2018]. Next are presented the main specifications of the Zephyr UAV. The data is from Zephyr 7, which at the time reached 21.000 of service ceiling and 14 days of unrefuelled flight (see table 2):

Chord	?*
Wingspan	22,5 m
Aspect Ratio	?*
Cruise speed	15,6 m/s
MTOM	53 kg
Engine Power	0,9 kW (0,45 kW each)

*No solid data of AR and of the chord

Table 2: Specifications of the Airbus Zephyr 7. From Wikipedia [c].

1.5.3 Environmental Impact

The major applications for HALE UAV happen to be communications and surveillance. The consequences of HALE UAV to the environment will be resumed as a comparison with the current systems that compete with them in this ambit — aircraft and satellites.

In the first place, solar powered UAV have demonstrated to have a lower cost compared to typical combustion aircraft and satellites. Besides, they release no emissions to the atmosphere, while combustion planes obviously do and most satellites also have an important ecological footprint when launched. It should be noted that at the altitude we are talking about (the stratorphere, as we'll see later on), there is no convection of gases and therefore any contaminant released in the stratosphere is likely to stay there for a long time, which may have uncertain effects on the climate.

Unlike satellites, they can land on their own for maintenance and be repaired. Satellites will be on orbit for years after cease of use, which creates a problem of space contamination, specially serious when talking about geostationary orbits. Solar powered planes have the obvious advantage that they leave no contaminants in the atmosphere as products of combustion. However, do they have zero impact on the environment?

Although we can certainly say they are much more beneficial for the environment than typical aircraft and satellites, we cannot forget to mention that solar powered UAV, like any other electric device, do have an ecological footprint on the planet. The plastics (and other materials) they are made of are widely known to be contaminant; they will stay in the same chemical state without decomposing for thousands of years. But we should put special attention elsewhere. Batteries, at their turn, are usually thought of the quintessential source of clean energy. But while they will for sure end up substituting fossil fuels (and improve the way we treat the planet), we shall not forget to pay attention at the way they are manufactured and recycled. Today we are rushing to extract all the possible amount of lithium from mines, which is turning into an environmental problem. Potable water can become contaminated in the process (as happened in the Tibet) and dry areas may become even drier because of intensive water use of lithium extraction (as happens in Africa).

To sum up, solar powered UAV do represent an improvement regarding environmental impact over typical aircraft and satellites, but we should not forget the materials they are made of, that they are not still fully green —fully recyclable—, so there's still some way to go. We must improve the way materials are extracted and reused afterwards.

2 Onboard Systems

2.1 Flight Control System

The Flight Control System (FCS) used will be based on the architecture proposed by the company *UAV Navigation*. This system mainly consists of an autopilot, a dedicated link to the ground station and other peripherals, mainly the actuators of the control surfaces. The FCS can also send commands to and monitor the propelling motors, batteries, solar panels, etc. This section will provide an overall view of the hardware involved in the FCS and of the main functionalities of each of the elements.

Autopilot

The hardware chosen is the VECTOR, an autopilot manufactured by UAVN (UAV Navigation). The Inertial Measurement Unit (IMU), a Global Navigation Satellite System (GNSS), an Air Data System (ADS), a barometric altimeter and a magnetometer come integrated with the autopilot, so it can on itself measure the position, velocity and the attitude of the aircraft. More importantly, it has single failure tolerance for all of the sensors, and multiple for some of them. Besides, it is prepared to withstand really high altitudes, as it comes encapsulated and can be pressurised to protect the most sensitive systems. However, note that although the altitude it can fly is the highest found on a Consumer Off The Shelf (COTS) product, it still won't be enough to fulfill the requirements of altitude of the UAV (see table 3 and section 3). The minimum sensing airspeed of 10m/s would also suppose a problem, as in landing or takeoff the velocity of the aircraft would be around 5m/s only — so the FCS wouldn't have a reliable input data for velocity.

Power consumption	2,5 W
Supply	9V to 36V
Weight	180 g
Dimensions	45 x 68 x 74,5 mm
Altitude	Up to ∼9km
Airspeed range*	10 - 128 m/s
Temperature range	-40ºC to +85ºC

*Range extendable to 23 - 231 m/s

Table 3: VECTOR's main features (from UAVN webpage).

Data Link

The data link chosen (TELEM05) is also manufactured by UAV Navigation, which is convenient because the required voltage input is the same, and so are the operating temperature and altitude ranges. The characteristics of the data link device that are more important to the design process are listed in table 4.

Actuators

Until the control surfaces of the wing are sized, we cannot know the size and required power of the propellers. However, in order to make an approximation for the Conceptual Design, a driver has

Supply	9 V to 36 V
Power consumption	6,5 W (peak)
Output power	1 W
Weight	180 g
Dimensions	108 x 85,2 x 31,75 mm
Temperature range	-40ºC to +85ºC
Maximum range	100 km

Table 4: TELEM05's main features (from UAVN webpage).

been chosen by rule of thumb. It is the model DA 15-N-ISS of the manufacturer Volz Servos. Its main characteristics are summarized in table 5.

Case Dimensions	29,4x39,4x14,6 mm
Weight	35 g
Arm length	7-23 mm
Voltage	6 V
Standby Current	0,05 A
Rated Current	0,5 A
Rated Torque	11 Ncm
Peak Torque	40 Ncm

Table 5: Specs of the driver motor DA 15-N-ISS. Obtained from [VOLZ] webpage.

2.2 Power Supply

Solar Panels

Table 6 shows the specs of *MicroLink*'s solar cells and solar sheets. There are some things to be mentioned about those products. First, the values taken for the design are those of the solar sheet, i.e. $350g/m^2$ of surface weight and 30% of efficiency under AM1,5 conditions. A brief aside: *AM (Air Mass) is a normalized number that counts how many atmospheres there are between the source of light and the solar device. AM1,5 is the value used for solar cells at the surface of the earth, 1,5 being the "mean" value of AM throughout the day. In space, we would be talking about AM0. The efficiencies of a single solar cells will be different under AM1,5 conditions and AM0 conditions because the spectrum of of radiation is fundamentally different; this solar cell would have a lower efficiency in space because, proportionally, it can gather a shorter part of the spectrum. However, this solar cell will still gather more energy in space than in earth because the amount of radiation in space is quite higher than at the surface.* This being said, the conditions at 16km of altitude are more similar to AM0 than to AM1,5, but the radiation data available in this thesis is from Earth's surface, so we'll take AM1,5 efficiency value (and we are still keeping in the conservative side).

Also to be mentioned is that the solar cells are flexible and can conform to curved surfaces, so it shouldn't be a problem to adapt them to the shape of the profile. Besides, the difference in weight between solar sheets and solar cells is due to a robust, waterproof package of the solar sheets. By now, this option is preferred, but there is the opportunity (for the future) of purchasing solar cells alone and designing a different, more lightweight package to improve the surface weight of $350g/m^2$.

SOLAR CELL	
Efficiency (AM1,5)	31%
Surface Weight	$< 250 g/m^2$
Dimensions	6,6x3,1 cm
Thickness	$40\mu m$
SOLAR SHEET	
Efficiency (AM1,5)	30%
Surface Weight	$350 g/m^2$

Table 6: Characteristics of triple junction solar cells and solar sheets (from MicroLink webpage).

Batteries

Sion Batteries provides the most energy dense batteries available. The batteries chosen for the design of the UAV have been the last generation Licerion® V2 cells, which will be available on the market soon and have a specific energy of 496Wh/kg. Its main characteristics are summarized in table 7. Besides, figure 1 shows other important specs of Sion's batteries, such as the discharge characteristics and the cycle life characteristics.

Nominal Voltage	3,82 V
Typical Capacity (C/3)	20 Ah
Nominal Energy	76,4 Wh
Weight	154 g
Dimensions	100x100x10 mm
Charge Voltage	4,35 V
Max. Charge Current	6,6 A
Max. Discharge Current	60 A (3C)
Temperature Range	-10ºC to 45ºC

Table 7: Characteristics of one 20Ah Licerion ® Cell.

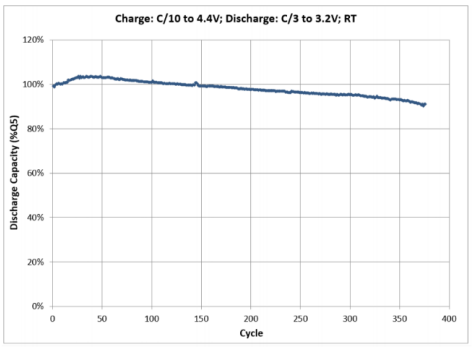

(a) Cell Cycle Life Characeristics.

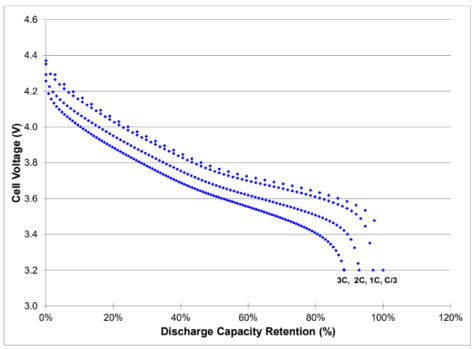

(b) Cell Discharge Rate Characeristics.

Figure 1: Other relevant specs of Licerion® 20Ah cells.

3 Environmental Conditions

This section will be devoted to choosing the design altitude and to explain what is the operating environment at this height. It is usual practice in engineering to use the ISA (International Standard Atmosphere) air properties for design purposes. It is in fact a valuable tool in many cases and the time required to calculate the environmental conditions this way is minimal.

However, the specific characteristics of this UAV made it difficult to rely blindly on such equations; they represent a good approximation for density and temperature at middle altitudes, though this is not so true at the poles or at the equator where the UAV will be operating. Besides, and more importantly, we should keep in mind that we are flying a Solar Powered UAV and that the primary goal of this thesis is to achieve infinite (theoretical) autonomy. This raises another problem, which is the dependency upon weather conditions; to solve this problem the aircraft should be able to fly above the clouds to assure a foreseeable radiation incidence pattern across the year.

3.1 Introducing the Stratosphere

The troposphere is the lowest layer of earth's atmosphere. It contains around 80% of the total mass of air of the atmosphere. The air is warmest in the bottom of the troposphere and it gets colder as one rises through this layer. The troposphere also contains most of the moisture of the atmosphere (the other layers are very dry in comparison) and most of the weather successes happen here, including cloud formation.

The stratosphere is the second layer of the atmosphere. The bottom of the stratosphere is called tropopause, which in a way acts as a separation between the troposphere and the stratosphere. The stratosphere is mainly characterized for a positive gradient of temperature; due to the heating of the ozone particles (relatively abundant in this layer) with the UV radiation from the sun, temperature increases with growing height. This temperature gradient rules the main dynamic properties of this layer of the atmosphere; due to this fact, there is a lack of convection so air is far quieter than it is in the troposphere. Commercial aircraft tend to fly in the lowest part of this layer to avoid the more common turbulence in the troposphere. The information provided above, as well as other pieces of interest, can be found at UCAR webpage.

For the reasons that will be explained just below, the Stratosphere is the ideal placement to fly a HALE UAV and thus our aircraft will fly at this height. The tropopause is a metheorological concept that defines the boundary between the troposphere and the stratosphere, two essentially different layers of the atmosphere. Although there is a more specific definition, a loose definition would be that it is the point where the air ceases to cool with height. Its height varies largely with latitude, and can go from 7-10km AMSL (Altitude Mean Sea Level) at the poles to 16-18km at the tropic [Mohanakumar, 2008].

From [Mohanakumar, 2008] and [Hoinka, 1998] it can be inferred that the tropical tropopause is at the 100hPa level, with a temperature of 192k and at an altitude ranging from 16-18km AMSL, being 18km more of an exceptional value. The UAV will be designed to be able to fly at the maximum altitude of 16km in order to benefit from the calmness and lack of weather of this bottom layer of the stratosphere.

Besides, being above the tropopause helps us avoid the Jet Stream. Jet Streams are fast flowing, narrow, meandering air currents in the atmosphere. The main Jet Streams on Earth are located near the tropopause and they may carry some trouble for aircraft flying at their altitude; as exposed

in Skybrary webpage: "Aircraft flying close to a Jet Stream may encounter Clear Air Turbulence (CAT) caused by Low Level Wind Shear [...] Not all jet streams are turbulent but aircraft exploiting the tailwinds afforded by a Jet Stream often experience light to moderate turbulence for much of the flight"

3.2 Radiation Incidence

Before estimating the size of the wings it is necessary to calculate the radiation incidence in a particular place and time. For design purposes, let's suppose the aircraft is situated on the equator (0^{o} latitude, 25^{o} longitude). As the aim is to fly the UAV the whole year, the time chosen for design will be the least favourable one, which on the equator happens to be June; figure 2 shows the radiation incidence for each hour of the average day of June. All the data regarding radiation has been obtained from the Photovoltaic Geographical Information System (PVGIS), which is an organization that gives public access to a great amount of experimental data about irradiation in different parts of the world. They have an interactive tool webpage (go to [PVGIS]) where this data can be consulted and downloaded. The data has been obtained specifically from the PVGIS-CMSAF database and is given at ground level and Clear Sky conditions.

The radiation at 16km is substantially higher than the radiation at the surface. There is a good amount of it that scatters or gets absorbed by air before arriving to the surface; the ideal would be to apply a correction factor to the surface data to obtain a realistic radiation profile at 16km. However, the author has not found a sufficiently good model to approximate the value of radiation at 16km of altitude from the values measured at the surface. Nicolai and Carichner [2010] provides values that suggest that radiation incidence may be around 25% higher at 16km, but the origin of this values is uncertain. Kaplani et al. [2018] provide a model for radiation incidence all around the globe and include a correction for altitude, but again the results for altitudes of the order of 16km aren't enough supported, and yield values of radiation $2,7$ times higher at the tropopause than at the surface, which seems to be a little exaggerated. For the reasons mentioned above, the analysis will be done with the empirical data obtained at the surface, while keeping in mind that is an approximation that stays in the conservative side.

3.3 Cloud Height

As said previously, it is important to know the distribution of the clouds with height in order to fly above them. It is of great importance to eliminate the dependence upon weather of the radiation incidence on the wing, as we are aiming at an UAV of infinite autonomy.

Cirrus clouds are the type of clouds that can be found at greater altitudes, as can be inferred from the dedicated [Wikipedia, a] webpage - apart from certain types of polar clouds, that can be found at greater altitudes. This type of clouds are characteristically thin, but are thought to be important regulators of the radiation of the planet [Sassen et al., 2008]. As can be seen in figure 3, Cirrus clouds are most frequently found in the tropics, so they are relevant to the location chosen to operate our UAV.

Figure 4 shows the averaged 1-year data of the height of the troposphere and the concurrence of cirrus clouds as a function of the height and latitude in earth. The troposphere, as said earlier, is around 16km at the tropics and at this altitude the frequency of cirrus clouds is of 10%. What is clear is that the area right beneath the tropopause should be avoided due to the high concurrence of clouds.

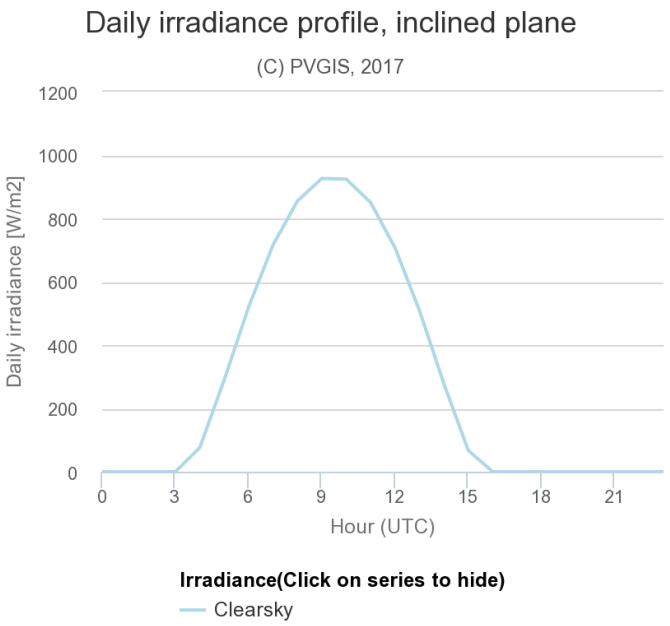

Figure 2: Average Incidence Radiation on June (0^{o} latitude, 25^{o} longitude)

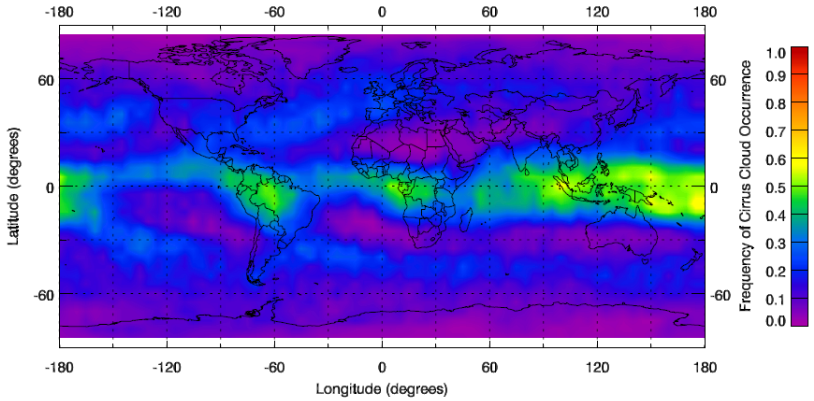

Figure 3: 1-year averaged measurement of frequency of ocurrence of cirrus clouds. Extracted from [Sassen et al., 2008].

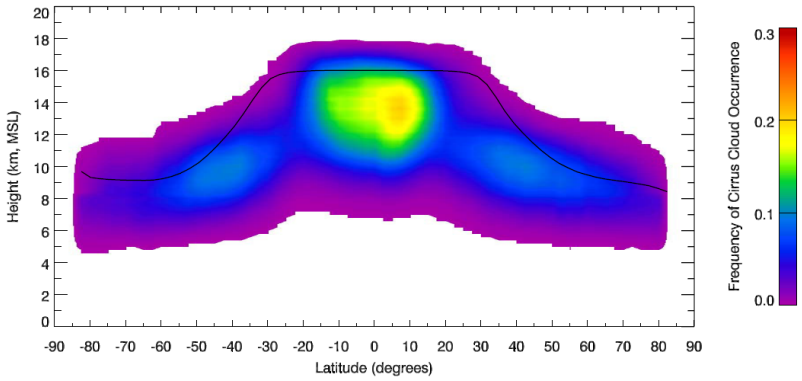

Figure 4: Latitudinal distribution of cirrus cloud heights. The black line shows the averaged tropopause height. Data averaged over 1 year. Extracted from Sassen et al. [2008].

3.4 Air properties

Recapitulating, the averaged height of the tropopause in the tropics is around 16km, the pressure about 100hPa and the temperature around 192K [Hoinka, 1998]. This will be the design height. We have seen that at such height the frequency of concurrence of cirrus clouds is around 10%; to avoid clouds completely, the ideal would be to fly at 18km, but 16km is thought to be enough. In this range of pressures the viscosity of air (considering dry air) can be calculated with Sutherland's law: its value at 192K is of $\mu = 12,83 \times 10^{-6} Pa \cdot s$. Sutherland's law is a particularly simple model to relate the viscosity of an ideal gas with its temperature. For air, Sutherland's equation adopts the form of eq. 1 (obtained from the web [CFD Online]).

$$\mu = 1,458 \times 10^{-6} \frac{\mathrm{T}^{3/2}}{\mathrm{T} + 110,4} Pa \cdot s \tag{1}$$

The density can be calculated with the ideal gas law, since we already know pressure and temperature, the only unknown is density — this yields a value of $\rho = 0,1815$.Furthermore, taking the cruise velocity equal to the Airbus Zephyr's (see section 1.5.2, i.e. roughly 15m/s) and venturing a chord of 0,75m this yields a Reynolds number of Re 160.000. The Helios prototype, developed under NASA's ERAST programme, has a greater chord and operates at Re $250.000 - 300.000$. Considering those two aircraft the expected Reynolds is between the $150.000 - 300.000$ range. This approximation of the Reynolds will be particularly relevant to choose a profile afterwards in the design process.

4 Conceptual Design

This section will set the basic parameters of our UAV. The idea is that every part of the wing will be as much "autonomous" as it can be, i.e. that one meter of wingspan will be able to generate enough lift to counter its own weight and enough energy to counter the drag energy losses, plus a little extra lift and energy to account for the weight and the energy of the Onboard Systems. The weight of the Onboard Systems is roughly fixed, so it is anticipated that there will be a minimum size of the wing so that the aircraft reaches a weight and energy balance.

The methodology of this section will be focused on finding an optimum design based on certain estimations found in the literature. Classic design books, like Torenbeek or Roskam, widely used to design all sorts of aircraft, do not apply to this case: mainly, because those books don't consider electric propelled aircraft, but also because the materials employed have changed substantially and the weight estimates are no longer of use. Besides, there aren't a lot of HALE aircraft nowadays, so the data available to elaborate empirical relations is sparse.

So some estimations have been made out of scientific papers on the topic, or recent investigations that time is yet to prove good or wrong. The risk is that these equations may not predict well enough the weight of unconventional aircraft, and therefore the optimization done in this section might not be so optimum. We'll keep this in mind for now and aftwerards, during the refinement of the design, the validity of the approximations employed here will be assessed.

The focus of this stage will be the to reach the Energy Balance, and the other parameters of design will be kept as simple as possible. The aerodynamics of the aircraft will be assumed to be like the aerodynamics of the wing and a bulk weight will be left to account for unknown masses (like the boom, the tail and undersized elements). Besides, the aerdynamic surfaces (wing, horizontal tail and vertical tail), will be kept rectangular; before doing any calculation, this seems a sensible thing to do because it keeps calculus simple, but also because the amount of solar cells would be less with the same wing area. The weight will be used as a rough indicator for price and manufacturability and we'll try to keep it as low as possible —that is, it will be the optimisation parameter.

4.1 Aerodynamics

Profile Choice

Unlike typical commercial airplanes, HALE UAV operate at Reynolds numbers between 50.000 and 500.000, the so called Low Reynolds regime. The flow in this range is fundamentally different than the flow at high Reynolds numbers. Under these conditions the boundary layer separates from the profile while being laminar, and then becomes unstable and makes the transition to turbulent flow in "mid-air", when it reattaches to the airfoil. This process generates the aerodynamic phenomenon called Laminar Separation Bubble, which comes with energy losses and is the main reason for performance deterioration in this regime.
Therefore, it is of great importance to use airfoils specially designed for the low Reynolds number range, specially to reduce the size of the laminar separation bubble. Donovan, Selig and Fraser carried a study to examine the effects of this bubble; it was summarized in the work [Selig et al., 1989], where the characteristics of 54 different airfoils are exposed, some of those designed by themselves. Most of the information on low Reynolds airfoils has been extracted from this book.
It is intended that the wing won't feature flaps or other high-lift devices, as they would increase the wing weight and complexity significantly; thus, the profiles that would need flaps have been avoided.

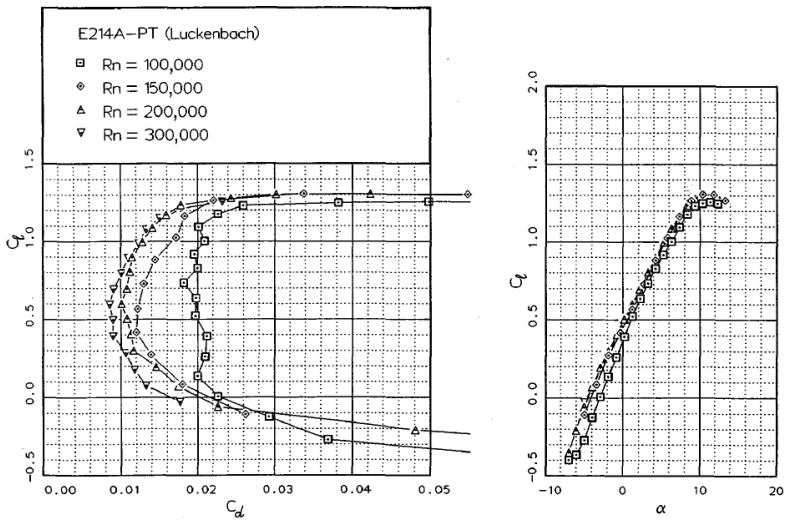

Figure 5: Polar and lift plot of the E214. Extracted from: Airfoils at low speeds, 1989.

Besides, special care should be put to those profiles with sharp stall; it would be dangerous to use them at cl's near the stall point. Finally, the shape of the profile has also been taken into account: too cambered or too slim airfoils may not be suitable to fit in the batteries and the structure.

Some airfoils are found to improve its performance at low Reynolds numbers (below 300k) when tripped, i.e. when a turbulator is placed at a certain place upstream of the laminar separation bubble [Selig et al., 1989]. However, those trips are useful for specific circumstances and may be disadvantageous in other conditions. So as long as this is a preliminary design, tripping the wing will remain a possibility for the future but won't be considered for the moment.

The first criteria has been to choose the profiles that had a better efficiency in the range of $Re = 150k - 300k$. Many of the airfoils weren't very good in this sense, specially approaching the lower limit of $Re = 150k$. Following this criteria, amongst the profiles listed in *Airfoils at low speeds* the four most suitable profiles were the SD7037, the SD7003, the E214 and the RG15. The parameter to be optimized here is the so called endurance parameter i.e. to optimize the propelling power needed we should aim to maximize the ratio $\frac{C_L^1,5}{C_D}$ instead of the more usual aerodynamic efficiency ($\frac{C_L}{C_D}$). Previous to the sizing of the wing all of them have their advantages and drawbacks; however, a sensitive choice can be made after a few trials with the methodology that will be mentioned below. The appropriate Cl is found to be around 0,6-0,7 and the Reynolds around $200k$. In this range, the angle of attack of the profiles is quite near the stall angle, and can be more when considering the induced angle of attack that accounts for the 3D wing effects. Therefore, the SD7037 and the RG15 are discarded because of their sharp stall. Between E214 and SD7003, the E214 has a higher endurance parameter (54 vs 46) but its average moment coefficient, as given by Donovan, Selig and Fraser, is ≈ 4 times higher. On the other side, the SD7003 is thinner and the batteries will probably have to be collocated horizontally instead of vertically, which will retard the center of mass.
Overall, it seems that the SD7003 will be the best option to reduce the size of the tail and will help cutting off the trim drag. The thickness of this profile is 8,51% of the chord and it has a light camber of 1,46% of the chord. The figures 5 - 8 show the polars of the four profiles considered at different Reynolds numbers.

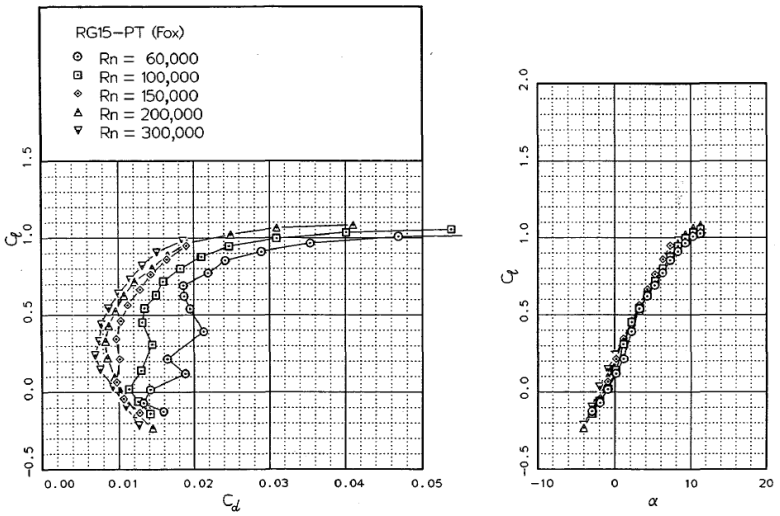

Figure 6: Polar and lift plot of the RG15. Extracted from: Airfoils at low speeds, 1989.

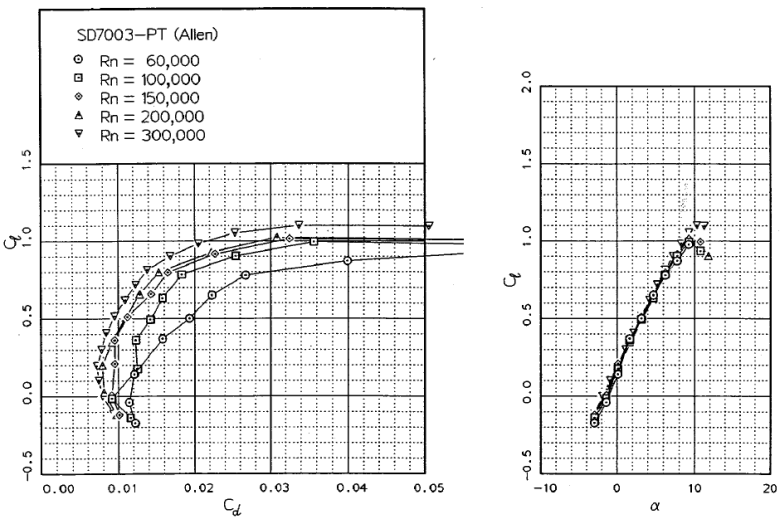

Figure 7: Polar and lift plot of the SD7003. Extracted from: Airfoils at low speeds, 1989.

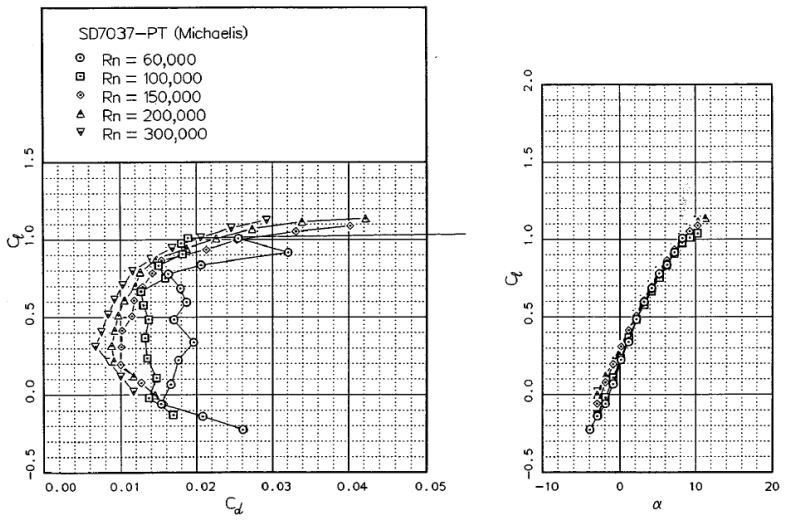

Figure 8: Polar and lift plot of the SD7037. Extracted from: Airfoils at low speeds, 1989.

Finite Wing

In order to account for the effects of the finite wing, the drag of the wing has been obtained the following way:

$$C_D = C_d + \frac{C_L^2}{\pi ARe} \tag{2}$$

Where C_D is the drag coefficient of the wing, C_d is the drag coefficient of the profile and where e accounts for the *span efficiency factor*, which should not be confused with the *Oswald efficiency factor*. The former accounts only for the loss of efficiency due to the wing planform and equals 1 for an elliptic wing. On the other hand, the Oswald factor accounts both for the variations of induced drag and parasitic drag due to lift [Anderson, 2017]. As this first approach is only focused on the wing and the parasitic drag due to the tail and the fuselage are not taken into account, here the Oswald factor isn't of interest.
The value of e was first computed theoretically by McCormick [1995]; the later expansion to greater values of AR has been obtained from Chen and Katz [2004] and yields a span efficiency factor of $e = 0,84$ when $AR = 26$, which would be similar to the value for airplanes like the Zephyr or the HELIOS, or $e = 0,89$ when $AR = 10$, which is more similar to the value of our airplane, as we'll see later.

Tail profile

As for the tail profile, the best option becomes to be the SD8020. It is a symmetric airfoil, but differently from other symmetric airfoils suitable for tail surfaces, it has a faster response near the zero angle of attack. Comparatively, the others have a lift curve which is almost flat near $\alpha = 0$ when Re $60k$, which yields a poor behavior when used as stabilizers [Selig et al., 1989]. This being said, NACA 0009 still stands as a good choice due to a slightly better L/D ratio at some points and a cambered profile could also be considered in certain situations.

4.2 Power estimation

Avionics

For this first approximation the only systems considered will be the autopilot, the data link and the servos used to drive the control surfaces. UAVNavigation provides the values for the autopilot (2,5W) and the data link (6,5W). 6,5W is the peak value, but we'll consider it for the sake of a conservative approach.
Regarding the drivers, we still don't know the requirements of power it will have, but as a first approximation the Volz servo DA-15-N-ISS will be chosen. Each of them weights 35g and consumes 0,3W (standby) and 3W (rated). Say it worked one tenth of the time, it would consume 2,3W.

Propulsion

The propulsive efficiency of the propeller is set, conservatively, to $\eta_p = 0,7$ as a first approach —similar aircraft have been seen to have much higher propeller efficiencies of 80% or even 90% [Noth, 2007]. The efficiency of the motor $\eta_{motor} = 0.97$, known to be a standard figure for Light Sport Aircraft (LSA) electric motors. Initially the gearbox losses won't be accounted for, but it is considered that the bulk efficiency given to the propeller absorbs the error.

4.3 Weight estimation

Avionics

We have set since the beginning of the design the avionics required for this project, and thus the weight of the avionics is well known. We saw in section 2 that the weight of the autopilot and the datalink is of 180g each; the servos (a total of four) account for around 140g. The weight of the servos is the only one that is variable, as the requirements of power of the drivers won't be calculated in this project and the real drivers needed can be either slightly heavier and more powerful or the other way around.

Solar Cells

The solar cells used will be those we talked about back in section 2: manufactured by MicroLink Devices, with a solar sheet efficiency of 30% (this figure considers the loss of efficiency due to packaging) and a surface weight of $350g/m^2$.

The usable area of the wing for solar cells is about 80% of the surface of the wing because a 15% of the chord, starting from the leading edge, shouldn't be used not to disturb the boundary layer; something similar happens with an additional 5% of the chord from the trailing edge. However, in order to account for the cells placed at the tail (that for now is not included in the design), we'll initially say that the surface of the solar cells is equal to the surface of the wing ($S_w = S_s c$) [Nicolai and Carichner, 2010]. A similar proportion uses the HELIPLAT UAV (see Frulla [2004]), although in this case the proportion of surface covered with solar cells to the area of the wing is more closer to 90%.

Batteries

As seen in section 2, the energy density of the batteries is of $\approx 500Wh/kg$. Their efficiency is not a value given by the manufacturer, so an approach will be made in this sense. We will consider an overall efficiency of 70%, which takes into account transmission losses, the consumption of a Power Control device and the trip efficiency of the battery itself Nicolai and Carichner [2010]. For calculus purposes, this efficiency will be divided into 83,7% entering and 83,7% going out of the battery.

Propulsion

The usual way to calculate the weight of the propulsion is the following. Taking empirical data from existing motors one can guess a ratio of Power/Weight. If we have such figure the weight of the propulsion can be put as a function of the necessary power to propel the aircraft. Noth [2007] did such analysis, and he gave also an estimation which also included the weight of the gearbox and the propeller. We'll take his estimation of 8kg/kW for a hand-launched UAV.

Airframe

The airframe weight is probably the most decisive factor for a good conceptual estimation and to define the shape of the wing properly. For the other components of the aircraft the weight is well known or can be put as a function of another variable. The airframe weight, instead, is usually calculated from data of similar aircraft, which in this case is a problem because there are few HALE UAV that rely on solar power for propulsion. In order to approximate the weight of the aircraft, once againg Noth's approximation has been taken [Noth, 2007]. He studies different generic functions that calculate the airframe weight as a function of S_W and AR and gives his own empirical approximation for HALE UAV of the type of Zephyr and HELIOS, that is the one we'll use here (see equation 3). As a warning for the reader, it should be noted that different approximations have been used, including those tested by Noth (and his own approximation), and none of them seems to be validated by the existing aircraft. It has been seen that the results obtained for the conceptual design are highly dependent on the estimation employed for the airframe. Anyway, over all the alternatives possible, Noth's seems to be the most specific one for the type of UAV that is being designed in this piece of work.

$$W_{airframe} = 0,022 \cdot S_W^{1.55} \cdot AR^{1.3} \tag{3}$$

4.4 Radiation Approach

As said before in section 3.2 the irradiation has been obtained from real irradiation data at ground level and in clear sky conditions. This data is given for an orientation of a solar panel of 0^{o}(plane tangent to earth's surface). Three main assumptions have been done here:

1. Nicolai and Carichner [2010] state that, not to disturb the boundary layer, the solar cells should start about 15% of the chord and for the same reason end at 5% of the chord. Besides, it is a sensitive approach to suppose that the tail will compensate for this unused space and, therefore, $S_W = S_{SC}$.

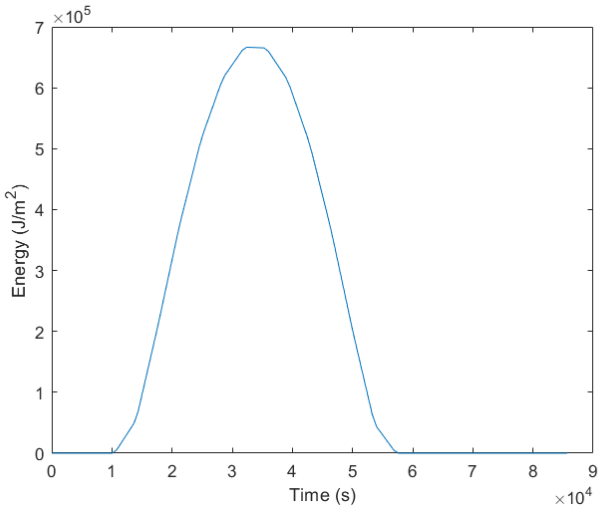

Figure 9: Energy per unit surface associated to each time step. Each hour has been divided in 5.

2. To all aspects, we are considering that the wing is a flat plate. Therefore, we are underestimating the weight of the solar cells by neglecting the curvature of the profile. This is not so ridiculous because there are no solar cells placed in the leading edge, the most curved part of the profile.

3. We will neglect the angle of attack of the profile when projecting the radiation incidence into the profile. For an angle of attack of 5^{o} $\cos\alpha > 0,99$, so this seems a sensitive approach.

A fourth assumption could be done here. That is: the irradiation decresases with decreasing altitude due to atmospheric attenuation. The real data collected gives the mean irradiation at sea level for a selected location, but the irradiation at 16km is quite higher. As said in section 3.2, once again, we've stuck to the conservative criteria; this correction has not been done because it was not possible to find a formal correction or a related study of the variation of radiation with height.

There are two codes related to radiation calculation, both of them can be consulted in the Appendix. *Integrate Radiation.m* (see the *Appendix* attached) receives the input data as power per square meter each hour (figure 2) and calculates the averaged energy per time step (figure 9).

We will define the *day* as those hours when the solar power alone is enough to provide the necessary power to the propulsion and the avionics. On the contrary, the *night* is the period when the batteries are providing energy, even though there might still arrive some radiation to the solar cells. *EnergySwitch.m* (see the *Appendix* attached) calculates the time when the *day* starts (t1) and finishes (t2). Then, t1 and t2 depend, not only on the amount of radiation of each day, but also on the power request of the aircraft. For the sake of exemplification, let's imagine two planes: the first one (A) of $1kg$ and $10m^2$ of solar cell area, and the second one (B) of $1000kg$ and $10m^2$ of solar cell area. Plane A and B both receive the same energy from the sun (they have the same amount of solar cells), but plane B isn't likely to receive enough energy to keep a levelled flight at any moment of the day, while plane A will. In our nomenclature, plane A will have a certain amount of *day* hours and *night* hours, but there will be no light at the end of the tunnel for plane B, who will be at a permanent *night*.

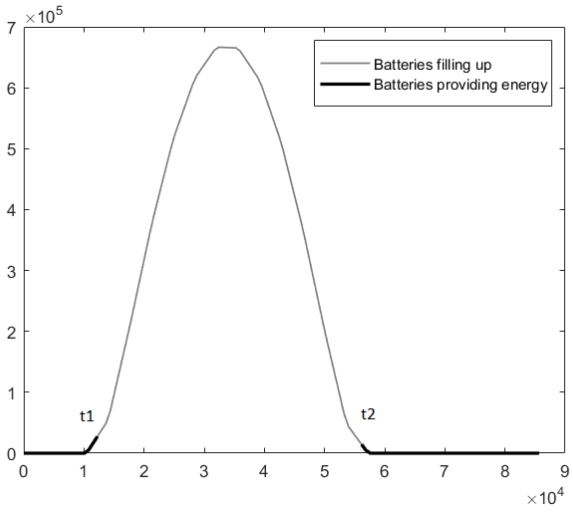

Figure 10: Point where the batteries switch giving/receiving energy. Time is in seconds and energy in Joules.

Then, t1 and t2 will depend on amount of power requested and the energy income from the solar cells. Figure 10 also shows how *EnergySwitch.m* function works.

4.5 Methodology

The aim was to obtain a planform wing that could generate enough lift to compensate the weight of the whole aircraft and at the same time obtain enough energy from the sun to power the motors and keep a levelled flight. For this first approach, the design variable will be the weight; we'll try to choose the option that minimizes the weight of the solution.
The aspect ratio (AR) and the surface of the wing (Sw) will be the design variables. We will give them values iteratively and see what is their effect on the final result. The velocity will be then chosen so that it minimizes the propulsive weight; this is the minimum cruise velocity for each configuration. For every couple of values (AR, Sw) the procedure is the following:

1. Calculate C_D with Eq. 2. Then the propulsive power is:

$$P_{propulsion} = D \cdot v = 1/2 \cdot \rho v^3 \cdot S_W \cdot C_D$$

2. Calculate the "constant" weight (only dependent on parameters and fixed variables like velocity, S_W and AR): the weight of the airframe ($W_{airframe}$) can be estimated through Eq. 3; the weight of the solar cells is proportional to the solar cell surface ($W_{SC} \propto S_W$), so it is also known; the weight of the avionics ($W_{avionics}$) is constant and known; finally the weight of the propulsion can be inferred from the calculated power ($W_{propulsion} \propto P_{propulsion}$).

3. Calculate the minimum energy of the batteries to keep a levelled flight during the *night* (equation 4

$$E_{batteries} = [(P_avionics + P_propulsion) \cdot (24 - (t2 - t1)) - E_{night} \cdot S_W \cdot \eta_{SC}]/\eta_{bat_{out}} \quad (4)$$

Where E_{night} is the energy provided by the solar cells during the *night*; η_{SC} and $\eta_{bat_{out}}$ have been defined previously and are the efficiencies of the solar cells and of the energy going out of the batteries, respectively. Then, we know the weight of the batteries because $W_{batteries} \propto E_{batteries}$.

4. Make sure, for each configuration, that the batteries receive enough energy during the *day* to be filled at t2.

5. Calculate the lift ($L = 1/2 \cdot \rho \cdot v^2 \cdot S_W \cdot C_L$) and make sure that it is greater than the weight.

Note that conditions 4 and 5 haven't been imposed; they have been checked at the end of the process instead. This has been found to be the best way to solve the problem computationally. In the first approach to the problem made by the author, the condition of balanced flight was imposed (L=W): adding one restriction took away one unknown of the problem, so the velocity was not an independent variable like it is now. However, the mathematical complexity and dependence upon variables augmented and, more importantly, the solution became too rigid: it only gave the balance solution for each AR and S_W. With the actually employed method the velocity is manually changed, but the display of the results is found much more useful: for a selected velocity, the factor $n = L/W$ of the aircraft can be plotted against AR and S_W, seeing directly the impact of those variables on the resultant weight and also seeing the configurations that are able to keep a balanced flight.

4.6 Results

Fig. 11 shows the evolution of the weight of the different subparts in which the aircraft has been divided. The following behaviour can be inferred. The different weights are always proportional to the wing surface. The weight of the airframe grows higher with increasing AR but the weight of the batteries and the weight of the propulsion decrease with increasing aspect ratios — due to a higher aerodynamic efficiency less power is needed, which has positive consequences on both variables—. So it is logical to think there will be an AR that is optimum, just before the weight of the structure becomes a too important fraction of the total weight. Note here that different approximations of the airframe weight will lead to different optimum Aspect Ratios for the same surface; it is a healthy thing we question the validity of the used approach here, because so much depends on it and at the same time we are beginning to obtain unexpected results. As seen from similar airplanes, it was expected to find aspect ratios of the order of 20, 25 or even greater, which has not been the case.

Figure 11a shows the "spare" lift for each combination of AR and S_W; the combinations that lay just on the striped line are equilibrated and the ones above the striped line can also carry some payload (or give room for some unknowns). Let define the "best" aircraft as the one that can carry most payload, based on Fig. 11a we can see that the best configuration is reached when $AR = 8$ and $Sw \approx 11m^2$. This yields a chord of $\approx 1,2m$ and a wing span of $\approx 9,4m$. However, as a first point we'll take $AR \approx 9$ and $Sw \approx 10m^2$ ($c = 1,05m$ $b = 9,5m$); the result is almost the same and it has been seen that in a situation of lower levels of radiation this configuration behaves better due to the higher Aspect Ratio. This configuration can carry a "spare" 5% of weight in this first design to make room for some unexpecteds. At its turn, it has also been checked that this plane was able to fill the batteries during the day. The flight Reynolds at cruise velocity and 16km AMSL is $\approx 200k$. The other features of the conceptual design aircraft are summarized in table 8.

Figure 11: Evolution of the weights of the aircraft as a function of Sw and AR

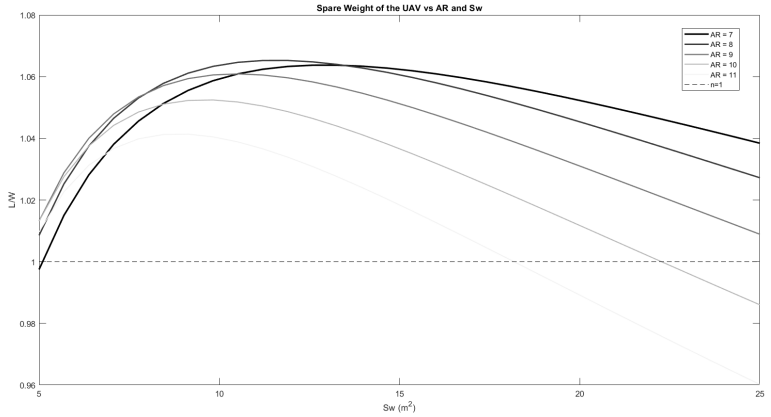

(a) Variation of L/W

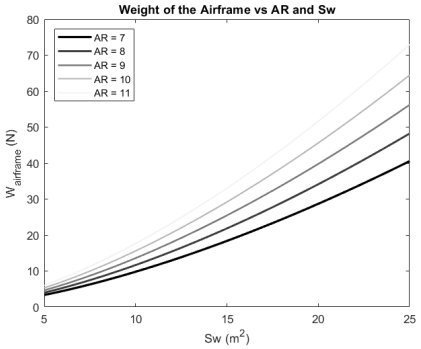

(b) Variation of $W_{airframe}$

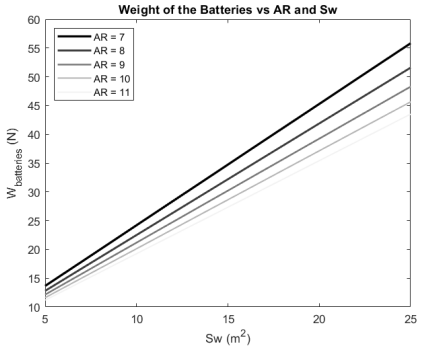

(c) Variation of $W_{batteries}$

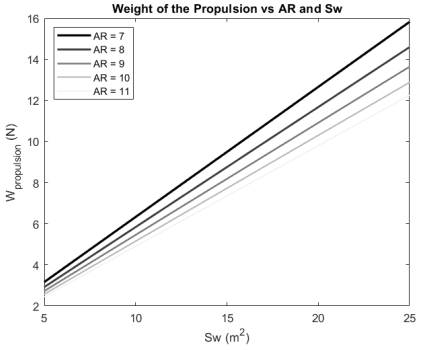

(d) Variation of $W_{propulsion}$

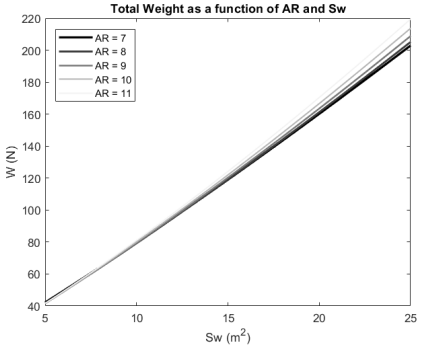

(e) Total weight of the UAV

Cruise velocity	12 m/s
C_L	0,645
C_D	0,0294
Chord	1,05 m
Wingspan	9,5 m
Total Weight	8,16 kg
Power consumption	80 W

Table 8: Aircraft characteristics at the Conceptual Design stage.

4.7 Tail sizing

Now that the planform shape of the wing has been defined, a tail should be also designed. In order to size the tail surfaces it is necessary to know precisely the center of gravity (c.g.) of the airplane. However, the c.g. location depends, among others, upon knowing the weight and position of the tail surfaces. Therefore, at this point we will use a method known as *Tail Volume Coefficient* approach, which is based on the observation that alike airplanes have similar tail volume coefficients [Nicolai and Carichner, 2010].

The vertical tail volume coefficient is defined as follows:

$$C_{VT} = \frac{l_{VT} \cdot S_{VT}}{b \cdot S_W} \tag{5}$$

Where l_{VT} is the distance between the c.g. and 1/4 of the vertical tail mean chord; S_{VT} is the lateral view surface of the vertical tail; b and S_W are already known parameters, the wingspan and the surface of the wing.

The horizontal tail volume coefficient is defined as follows:

$$C_{HT} = \frac{l_{HT} \cdot S_{HT}}{\bar{c} \cdot S_W} \tag{6}$$

Where l_{HT} is the distance between the c.g. and the quarter of the chord of the horizontal tail; S_{HT} is the planform area of the horizontal tail; $\bar{c}$ is the mean chord of the wing, which for a rectangular wing as ours is the same as the chord ($\bar{c} = c$).

We'll assume that $C_{VT} = 0,022$ and $C_{HT} = 0,5$. These values have been extracted from Nicolai and Carichner [2010] and come from sailplanes' data. Since sailplanes need to manoeuvre much more agressively than HALE UAV do, it is probable that this first approximation will yield to an oversized tail, though this is the best reference available at the moment.

For the following analyses of the tail, the criteria employed will be of stability during cruise i.e. values of $C_{n\beta} > 0$ and $C_{m\alpha} < 0$ will be looked for, but at the same time trying to keep trim drag low. Namely, the drag produced by the tail action should be kept, as a reference, under 10% of the total aircraft drag [Nicolai and Carichner, 2010]. Bigger tails lead to improved stability but the resultant trim drag is unacceptably high.

4.8 Aerodynamic validation

The aerodynamic assumptions previously made shall be validated now, manily, the 3D wing correction and the assumption that the total aerodynamic behaviour of the aircraft would be very similar to that of the wing alone. However, at this point of the design the center of gravity is still unknown, so the exact positioning of the tail can only be approximated and the stability assessment cannot be done yet.

Nonetheless, a sample tail has been chosen taking into account the tail volume coefficient approximations made just above, which enables to estimate the total drag and gives a start point for the iterative process of the tail design. The validation of the drag will allow, in the first place, to choose an electric motor that fits the airplane.

This validation has been made with the open software XFLR5 v6.46. This programme uses the Vortex Lattice Method (VLM) and the Lifting Line Theory (LLT) to give approximations for 3D wings. The LLT method has given trouble for the imposed conditions, so the chosen method has been the VLM. The VLM typically forgets about the viscous drag to account only for the effects of the induced drag. At low Reynolds conditions, as is the case, this is unacceptable; to solve this, XFLR5 interpolates from 2D empirically-corrected data from Xfoil to account for those effects. As there is no theoretical or experimental solid background to support the validity of this interpolation, it should be used carefully [XFLR5, 2013]. While this seems to have sense and overall XFLR5 gives good enough results for a first approximation like this, special care has to be taken when the Reynolds number is too low (note that Re is $178k$ for the wing but it can be as low as $64k$ for the vertical tail).

Figures 12 and 13 are screenshots of the results from XFLR5. This results come from the ring vortex VLM approximation ("VLM2" in the programme) with tilted geometry. Although the classical horseshoe vortex ("VLM1") offers similar results at a much reduced time toll, the visualisation of the induced drag showed several important discontinuities, which meant that its results could not be fully trusted. The physical characteristics of this analysis are registered in table 9. $\Delta\alpha_{wt}$ being the difference between the angle of attack of the wing and the tail.

Figure 13 shows the relevant aerodynamic plots when the wing and the tail have 0 relative angle of attack. Although this is unlikely, it has been seen that a difference of -5º would change very little the lift and drag characteristics and the plane and would only have a major role in the moments plot. Most importantly, it should be noted that the results obtained are very similar to those predicted by the Matlab programme: when $C_L \approx 0,65$, XFLR5 yields a $C_D \approx 0,03$ which is the same result obtained for the analysis of the wing alone in the Matlab programme (table 8). Therefore, the aerodynamic drag obtained from the Matlab programme is corroborated. Nonetheless, we will keep in mind that XFLR5 tends to subestimate the drag when chosing a motor for our aircraft.

$\mathbf{b_w}$	9,5 m
$\mathbf{c_w}$	1,05 m
$\mathbf{l_{wt}}$	4,75 m
$\mathbf{b_{ht}}$	2,57 m
$\mathbf{c_{ht}}$	0,43 m
$\mathbf{b_{vt}}$	1,15 m
$\mathbf{c_{vt}}$	0,38 m
$\mathbf{\Delta\alpha_{wt}}$	-2,7º

Table 9: Physical Characteristics of the plane; Conceptual Design configuration.

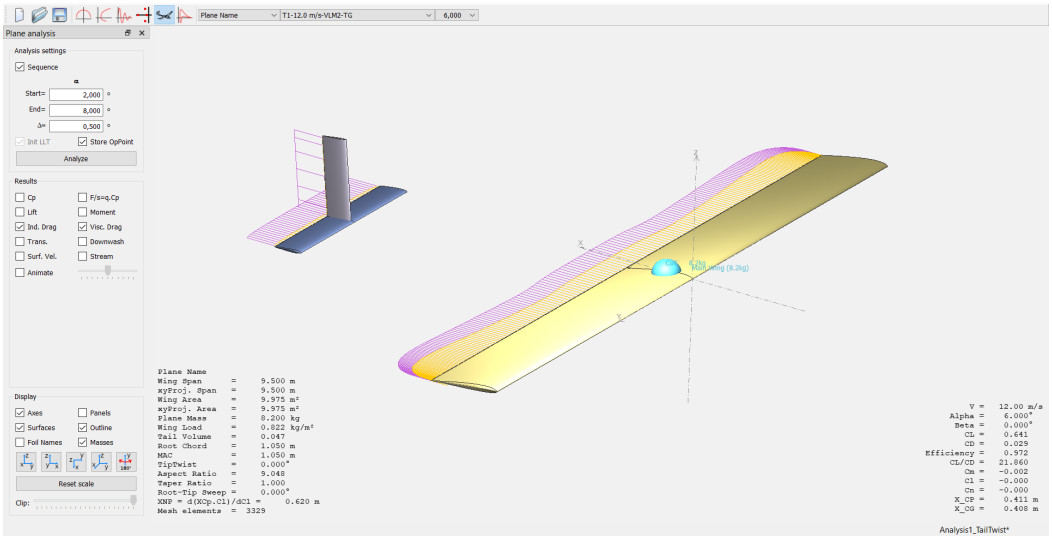

Figure 12: Screenshot of the XFLR5 representation of Configuration 1. Viscous drag is represented in purple and induced drag in yellow.

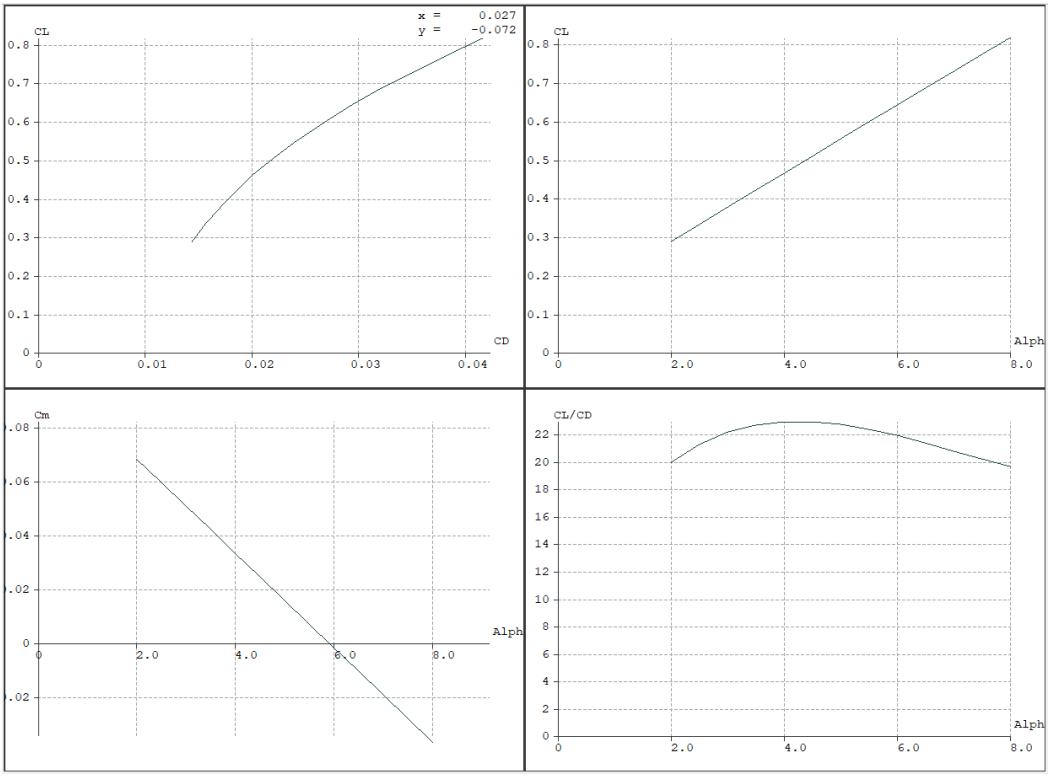

Figure 13: Aerodynamic plots for Configuration 1. Obtained with XFLR5, ring vortex VLM with tilted geometry.

5 Aerodynamics

After having defined the planform shape of the wing in section 4, now we'll focus on refining the design of the plane. This aerodynamic section, specifically, will be aimed at finding a suitable tail for the plane and to have defined the main aerodynamic coefficients of the plane as a whole: the C_L, C_D and C_{M_α}. This calculation has been carried on concurrently with the Structural design, as every change in the tail position or its size affected the center of gravity and viceversa, and also with the final sizing of the propulsive plant.

5.1 Stability Criterion

The direct parameter that indicates stability is the coefficient C_{M_α} — if this coefficient is negative the aircraft will be stable in front of aerodynamic perturbations (it will tend to return to its original equilibrium position), while a positive C_{M_α} means an unstable configuration for the plane and when this coefficient is zero the aircraft is neutrally stable. Typical values of C_{M_α} range from -0,0035 1/° (fighters) to -0,028 1/°(commercial aircraft). A small aircraft like Cessna 182 has a C_{M_α} of -0,014 1/° [Nicolai and Carichner, 2010]. As for our UAV, a guess is that -0,007 1/° should be enough. For this preliminary design, though, the value will be more close to the typical values of small aviation aircraft, like the Cessna.

The **Static Margin** is an indicator of the stability of an aircraft alternative to the derivative of the coefficient of pitching moment. If it is positive it means that $C_{m_\alpha} < 0$ i.e. that the aircraft is stable, whereas a negative value indicates that the aircraft is unstable in front of aerodynamic perturbations. If the Static Margin is 0 this means that the Center of Gravity is coincident with the Neutral Point, which is by definition the position where $C_{M_\alpha} = 0$ and so the aircraft will be neutrally stable. The Static Margin (SM) is defined as follows [Nicolai and Carichner, 2010]:

$$SM = \frac{NP - x_{cg}}{c_w} \tag{7}$$

Where NP and x_{cg} are the positions of the Neutral Point and the center of gravity of the plane, repectively; c_w is the chord of the wing.

5.2 Typical tail vs T tail

A study has been carried in order to determine whether the T-tail configuration is worth considering or not comparing it to a typical tail configuration and leaving all the other paremeters equal. On one side, it is known that the T-tail allows the tail out of the disturbed flow of the wing and therefore it provides better control of the aircraft and more predictable design characteristics. On the other side, a T-tail gets the tail out of the slipstream of the propeller of the aircraft, which could be detrimental. A T-tail usually brings deep stall problems too, although this is not so relevant for the design of this UAV. Finally, a T-tail configuration usually means an increase of the weight of the vertical tail, as it needs to be tougher to withstand the aerodynamic forces of the horizontal tail.
It is very difficult to measure the effects of the propeller wake at this moment, and so its effects won't be considered yet. However, we can study the effect of the wing wake alone and take a decision from the gathered data.

As can be appreciated in figures 14a and 14b, the gain in efficiency is (at $\alpha = 0$) not that much between a T-tail and a typical tail: $EC_L/C_D = 22,221 \rightarrow 22,167$. However, the difference is more important when looking at the stability: $C_{M_\alpha} = -0,788 rad^{-1}$ for the T-tail and $C_{M_\alpha} = -0,702 rad^{-1}$ for the typical tail configuration. This implies a 12% more stability, in a way, when using a T-tail compared to a typical tail.

The trim angle of attack of the tail is also different for the two configurations: 3,5° for the T-tail and 3,77° for the typical tail configuration.

So what can be gathered from all this is that an elevated tail will provide more stability than a non-elevated one if they are the same size (with similar efficiency). Another way to see it is that for a specific aimed C_{M_α} the size of an elevated tail will be smaller than a non-elevated one, thus increasing the overall efficiency of the plane.

5.3 Final Configuration

The final configuration will have a T-tail, for the reasons expressed in section 5.2, exactly the one showed in figure 14a. The profiles of the wing and the tail have been kept the same as in the conceptual design: that is, the SD7003 for the wing and the SD8020 for the tail. The other relevant aerodynamic parameters of the plane are summarized in table 10, and can also be consulted in the *Technical Sheets*. Note that l_{wt} refers to the distance between the aerodynamic centers of the wing and the tail.

$\mathbf{C_L}$	0,645
$\mathbf{C_D}$	0,029
$\mathbf{C_{M_\alpha}}$	-0,01375 1/°
$\alpha_\mathbf{w}$	6°
$\alpha_\mathbf{t}$	3,5°
$\mathbf{C_L/C_D}$	22,22
$\mathbf{x_{cg}}$	0,42 m
$\mathbf{l_{wt}}$	4,75 m

Table 10: Main aerodynamic parameters of the final configuration.

Some other things are to be mentioned. First, that the tail drag supposes a 10,43% of the total

Figure 14: Viscous (purple) and induced (yellow) drag for two different tail configurations

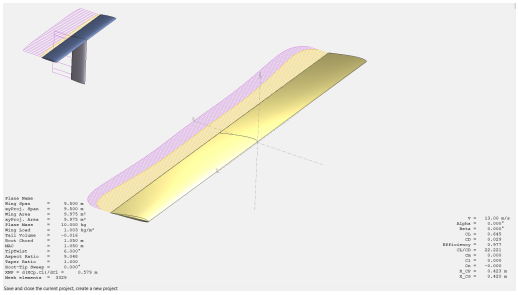

(a) Drag of the T-tail configuration.

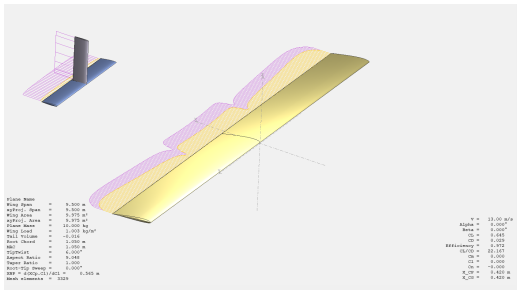

(b) Drag of the typical tail configuration.

drag in cruise conditions. 9,91% is due to the drag of the tail alone and the rest is the drag due to the interference between the wing and the tail. Nicolai and Carichner [2010] says that values of tail drag due to the trim load on the tail should not exceed 10% of the total drag in cruise conditions. The final configuration of this preliminary design is just over the limit, then, and this should be improved in further refinements of the design. Another way to see this is with the static margin, mentioned in section 5.1: for the chosen configuration, the center of gravity is located at 0,42 m from the leading edge of the wing ($x_{cg} = 0,42m$) and the analysis with XFLR5 have yielded a value of the Neutral Point of 0,58m, which gives a Static Margin value of $\approx 15\%$.

Therefore, the aircraft is now more stable than considered neccessary. One idea to reduce the trim drag would be to move the c.g. aft. A c.g. moved backwards allows the wing to counter in part its own pitching moment, so the tail can be smaller. The side effect of this is that the $|C_{M_\alpha}|$ is reduced (i.e. the stability is reduced), but this could be a price to pay willingly in our case.

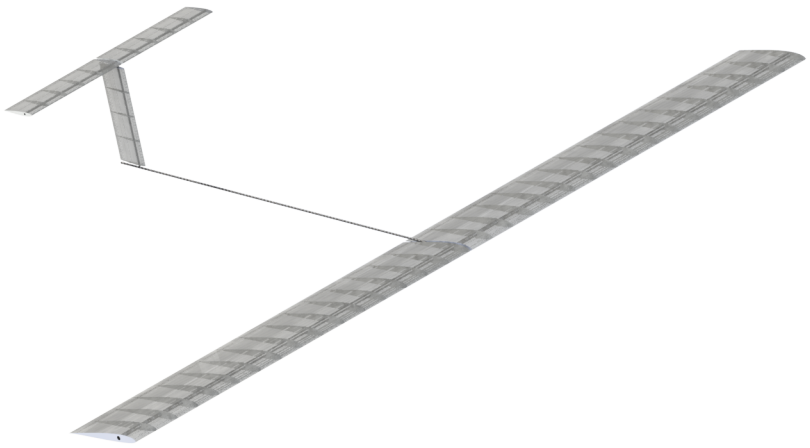

Figure 15: CAD representation of the structure of the UAV.

6 Structure

This section presents the final structure and layout of the UAV. The structural design has been done together with the aerodynamic calculations in order to obtain a configuration that would assure static stability in the longitudinal axis, because any change in the center of gravity affects the design of the tail and viceversa. Besides, the propulsive weight has also entered the iterative deign. The changes relative to the Conceptual Design can be seen in section 6.5.

The shape of the aircraft has been kept simple for several reasons (namely, the wing and tail are rectangular, without dihedral and unswept); this is mainly to avoid making idealistic design assumptions and to keep the hypotheses as simple as possible. Some design considerations, such as a tapered wing, could improve substantially the performance of the aircraft, but the structural implications this would have are not well known, apart from the reduction of the effective area to place solar cells, and thus the decision has been to avoid muddy water.

6.1 Layout of the structure

This section intends to explain the overall functioning of the structural design, the paper that each element takes in the whole picture, and also what has designed as part of this Preliminary Design and what is left to be developed in further studies. Also say that the structure design has been inspired from those proposed by Hibbs et al. [1998], Nicolai and Carichner [2010] and Frulla [2004]. Finally, comment that in this second stage of the design (the concurrent structural-aerodynamics design) the flight velocity has been updated from 12m/s to 13m/s to generate enough lift.

First of all, we can see a CAD of the structure in figure 15 made with the software Solidworks. The main elements that have been considered in the design are the ribs and the skin, to keep the desired shape of the profile, and the spars (the boom is considered a spar also).

The three aerodynamic surfaces share a common idea of structure. There is a tubular main spar made of CFRP (Carbon Fiber Reinforced Polymer), namely carbon fiber impregnated with epoxy

resin, that supports most of the stresses. Then the skin and a number of ribs together conform the shape of the wing. Because the ribs are very thin and won't be able to withstand lateral loads, a trailing edge spar is incorporated in order to prevent them from bending in the spanwise direction.

What has not been designed are the supports for the solar cells, as it is understood that the skin alone is not capable to withstand the weight of the solar cells as well as the aerodynamic forces. Two ideas in this direction would be to hold the solar cells with a structure made of foam (or just pierced foam panels) and to wrap the solar cells between two layers of skin material to keep them in the desired place[Frulla, 2004]. Also, it is of great importance to keep the shape of the leading edge, as a good part of the aerodynamic behaviour of the profile depends on it. Thus, it may be good idea to play safe and increase the amount of ribs in the front part of the profile, which also gives the advantage that the batteries can be located in the front part of the wing, held by two pieces of foam. This option, though, has not been included in the CAD yet and a structural-aerodynamic analysis of the skin (necessary to validate its thickness) has not been implemented. Most of the weight these elements add is thought to fit within the bulk weight left in the design, although there is the possibility that those elements, along with other electrical components, the payload and the fittings to join structural parts may exceed this bulk weight, and therefore the whole design should be rethought. However, the author is of the opinion that there is plenty of room to make small changes in the actual design.

6.2 Airframe

6.2.1 Ribs

The material employed for the ribs is a lightweight rigid foam based on polymethacrylimide (PMI). The specific foam chosen has been the ROHACELL® HERO, which is quite lighter than the widely used balsa wood in this kind of applications. The most oustanding feature of this product is its damage tolerance, meaning that it can be highly deformed before collapsing. The relevant properties of this compound are summarized on table 11 and can also be consulted at [ROHACELL] webpage.

Density	52 kg/m^3
Compressive Strength	0.6 MPa
Compressive Modulus	32 MPa
Tensile Strength	2.6 MPa
Tensile Modulus	82 MPa
Elongation at Break	8%
Shear strength	0.7 MPa
Shear Modulus	22 MPa

Table 11: Relevant physical characteristics of the ROHACELL HERO.

The ribs have been given a thickness of 2mm each. The profiles have been spread equally through the wing with a separation of (at least)30cm among profiles. An increase in number of ribs in the LE zone, as mentioned earlier, would allow the skin to keep the desired shape so that the aerdynamic properties of the real wing are as equal as possible to those of the calculated wing.
The criteria of separation and thickness of the ribs has been the same for all the aerodynamic surfaces.

6.2.2 Skin

For the skin, HOSTAPHAN® film has been chosen. Its density is $\rho = 1400 kg/m^3$ and a thickness of $25\mu m$ will be used, which yields a weight per unit surface of $35 g/m^2$. The other relevant properties of HOSTAPHAN film can be consulted at table 12 and at [Mitsubishi Polyester Film] webpage.

This thickness value applied is arguable and should be for sure discussed in any further analysis of the UAV. One should ask whether the skin has the permeability and thermal insulation necessary for this type of UAV; such analysis is off the scope of this project and therefore won't be discussed further. Previous to the structural analysis, there is no real clue about the thickness the skin should have, so the criteria employed is a kind guess of the author. Afterwards, in the structural analysis, we'll try to validate if this guesses are correct, although it might be difficult to do so with the skin.

Density	1400 kg/m^3
Impact Resistance (longitudinal)	1400 kJ/m^2
Impact Resistance (transversal)	1800 kJ/m^2
Coefficient of friction	0,4

Values measured on a $12\mu m$ thick film

Table 12: Relevant properties of HOSTAPHAN® film.

6.2.3 Spars

As can be seen in the structure layout (see the attached document *Drawings*), the wing box will be composed of two spars. One main spar that will withstand almost all the loads and torques applied to the wing, and a second spar whose function is to ensure the structural stability of the wing — that is, to prevent the ribs from bending or rotating around the main spar. The main spar will be collocated at 25% of the chord and the secondary spa will be at the trailing edge of the wing.

A Carbon Fiber Reinforced Polymer (CFRP) will be employed as main structural element to bear with stresses. Namely, the M60JB product from Toray Composites will be employed both in the spars and the boom. Toray Composites is a leading manufacturer in the ambit of composites, having a key paper on the development of modern composite-manufactured aircraft. The M60JB is a carbon fiber prepreg product which outstands for its high stiffness. It has a density of $1460 kg/m^3$ and a typical thickness of 0,9mm. The other important characteristics of the prepreg fiber are summarized in table 13 and can be found also in [Toray Composites] webpage in the section of prepreg products.

6.3 Non-structural Weight

Although the batteries and solar cells aren't obviously structural components, they will be commented here as an important part of the weight and therefore as key contributors to the location of the center of gravity. The amount and total weight of the batteries and the solar cells has changed since the Conceptual Design for the reasons that will be explained now.

Carbon fiber content (Wf)	80%
Resin Content (RC)	20%
Resin Type	Epoxy
Density	1460 kg/m^3
Tensile strength*	2,010 MPa
Tensile Modulus*	360 GPa
Tensile Strain	0,55%
Compressive Strength*	790 MPa
Flexural Strength*	1,07 MPa
Flexural Modulus*	301 GPa

*Values normalized to 60% fiber volume.

Table 13: Physical properties of M60JB Toray's CFRP.

6.3.1 Batteries

Having updated the structural weight, the design velocity needs to be higher and as a side effect the power required to fly is also increased. Therefore, the weight of the batteries increases from $21,1N$ to $26,2N$. For a real, discrete number of batteries this means that we would need at least 18 *Licerion* batteries.

However, we have to take into account that the propulsive efficiency has also lowered, which means that to provide the same thrust now the electric motor is consuming more energy, and thus we need more batteries. Considering a propulsive efficiengy of $\approx 60\%$ (see section 7), the necessary energy to fly all night is of 1528Wh, which accounts for 20 *Licerion* batteries (3,08 kg of batteries).

6.3.2 Solar Cells

From what has been gathered of solar cells, some observations can be done:

1. They represent a very important part of the total weight of the aircraft
2. In the equator the assumption $S_{sc} = S_w$ does not have a lot of sense: there is plenty of solar energy available and the weight of the solar cells is quickly too important to add more. Few solar cells are needed under this conditions and the wing area doesn't need to be completely covered.
3. After observation 2, the Conceptual Design may need to be revised. If the area covered by the solar cells was the minimum required by the circumstances (and not the maximum available), the combination of AR and S_w that was best before need not be the optimum configuration now.

After taking those points into account, the total surface of the solar cells is set to 70% of the wing surface. Under the light conditions in the equator, the aircraft will still collect far more energy than the needed, which yields the possible energy required by the payload. It should be mentioned that the cells are placed the nearest to the leading edge the possible (i.e. from 15% of chord to 85% of the chord); this brings the cg forward which helps reduce the tail size. For this same cg argument no solar cells have been placed in the tail.

6.4 Weight Refinement Methodology

In this section the calculations made in order to refine the weight estimation will be explained, as well as the ones to find the center of gravity of the UAV. Those calculus are necessary for two reasons: first, to validate the approximations made in section 4; and second, knowing the center of gravity is essential to fix a size and position for the horizontal tail, which at the time will let us know the stability characteristics of the plane. Note that only the x position of the center of gravity will be relevant in this stage of the design. The y position of the weight is almost nonexistent apart from the contribution of the vertical tail.
For all the center of gravity related calculus, the formula for n discrete elements is the following one:

$$\begin{cases} x_i = \frac{1}{M} \sum_{i=1}^{n} x_i \cdot m_i \\ M = \sum_{i=1}^{n} m_i \end{cases} \tag{8}$$

Where x_i and m_i are the position and mass of the i element respectively. M is the total mass of the system.

Skin

A data file containing the discrete points of the profiles employed can be found at [Airfoil Tools] webpage. First the perimeter of the profile is calculated adding up the distances between neighbour points; this yields a perimeter of roughly two times the chord of the profile. Then this perimeter is multiplied by the design thickness of the skin and the span of the aerodynamic surface. This gives the best approximation that can be obtained with the accessible data.

For the center of gravity calculation, equation 8 has been employed. The x position of the c.g. (x_{cg}) of the skin gets to be $0,495 \cdot c$ and the y position (y_cg) is roughly 1%c, so it will be neglected for simplicity.

Ribs

To calculate the area of a rib, the profile has been divided into trapezoids. Then the total area of the profile can be computed using equation 8 adding up the areas of each trapezoid. The x_{cg} of a rib is $0,388 \cdot c$ and the y position of the cg can be neglected as before ($y_{cg} \approx 2\%c$). Note also that it may be a good idea to pierce the ribs, which would mean that the real weight of them is lower than the provided by this calculus, which is therefore still an estimate.

Spars

Regarding the main spar and the trailing edge spar of each aerodynamic surface, the calculus have been very simple. We already have the thickness of the CFRP (0,9 mm) and the total length of the spars (equal to the span of each surface). Then, we only need to define the diameter of the main spars and the width of the TE spars to have the volume of material employed and therefore the weight. Remember that the dimensions of each spar can be found in the correspondent attached document of *Drawings*.

6.5 Center of Gravity

In this section all the masses and positions of the different elements of the UAV will be gathered, and the final Center of Gravity position will be calculated; it is a parameter of great importance in the aerodynamic study that has been done at the same time.

The reader will see that there may be slight changes from the values given in this section and the values given in the structure layout and the attached *Drawings*. These changes are few and do not change the center of gravity location significantly. To give an example, the number of ribs has increased in two units in order to give room for the boom and the piece that should fix it to the main spar and at the same time keep the minimum space between ribs of 30cm that has been fixed. Also, the length of the boom would need to be a little bit longer than the distance between spars in order to join the boom and the spar properly.

Element	**Mass**	**x position**	**y position**
Airframe	2,28 kg	1,16 m	0,12 m
Propulsion	0,89 kg	-0,05 m	0 m
Solar Cells	2,44 kg	0,53 m	$\approx$ 0,05 m
Batteries	3,08 kg	0,06 m	0 m
Avionics	0,50 kg	0,06 m	0 m
Payload/ Bulk Weight	0,81 kg	0,06 m	0 m
TOTAL	**10 kg**	**0,42 m**	$\approx \mathbf{0,04m}$

Table 14: Breakdown of the c.g. calculation of the UAV

Element	**Mass**
Ribs	0,22 kg
Spars	1,09 kg
Skin	0,82 kg
Boom	0,15 kg
TOTAL	**2,28 kg**

Table 15: Airframe mass breakdown.

Element	**Mass**	**x position**	**y position**
Wing	1,84 kg	0,40 m	0 m
Horizontal Tail	0,20 kg	5,07 m	1,15 m
Vertical Tail	0,09 kg	5,04 m	0,58 m
Boom	0,15 kg	2,98 m	0 m
TOTAL	**2,28 kg**	**1,16 m**	**0,12 m**

Table 16: Breakdown of the c.g. calculation of the Airframe.

The position of the airframe is a product of the structural needs and has little room for change. The propulsion position is a mere estimate. All the other components can be moved with certain freedom and they are located as near the prow as possible to move the center of gravity forward.
As for the y position of the c.g., note that it is really small. Although we cannot just say that the

effect ofy_{cg} is negligible, as long as this can entail a contribution of the motor to the equilibrium of moments, it is in fact very easy to counteract it with slight changes in the position of the motor, the boom, etc. so we'll work as if its effect were non-existent.

6.6 Structural Validation

In order to validate the structural stiffness of the design a computational analysis has been carried out. While the optimum at this point would be to make an analysis of the whole structure (including spars, ribs and skin), this has given some computational trouble because of the small thickness of some elements like the spar or the skin. Therefore, for the moment we'll test only the behaviour of the spar, which is the element that will bear with most of the stresses imposed to the structure. In order to validate the design of the ribs and the skin some deeper analysis should be made around the shape of the profile (like a CFD), which is out of the scope of this text.

The boom and the tail spars won't be bearing with high stresses. The one structural element that has to be tested is the main spar of the wing. In order to determine if the diameter and thickness of it are enough to withstand the aerodynamic and weight forces, the spar has been tested with the software Solidworks the following way: a semispar has been fitted at one end and at the other a force of 49,05N (half the weight of the plane) has been applied.

This is a simple analysis that simulates the situation of the plane hanged on its wing tips (if the weight was concentrated at the middle). It is a simple analysis and provides a security factor, as this is a load much higher than the plane main spar would need to withstand in any flight situation. The results of this analysis are shown in figure 16; as it is shown, the highest stresses at the end of the spar are one order of magnitude lower than the maximum tensile strength. (Note: the elastic limit "límite elástico" in the image corresponds to the maximum tensile strength). The maximum displacement at the tip of the spar is around 16cm, which is a rather good value as it represents only an angle of $2^{\underline{o}}$ of deviation from the horizontal.

Figure 16: Structural Analysis along the semispar of the wing; 49,05N applied at the tip.

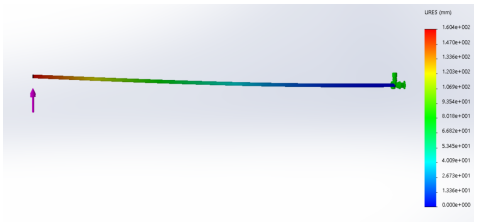

(a) Representation of the displacements.

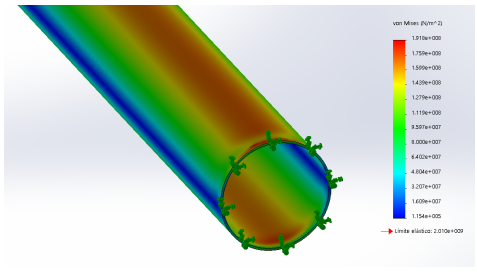

(b) Representation of the stresses.

In figures 17a and 17b can be seen, respectively, a representation of the mesh employed for the analysis and a screenshot (in Spanish) of the mesh details. Note that it is a rather thin mesh; because of the thickness of the CFRP layer (of 0,9mm) the mesh had to be this thin, which caused some computational trouble and made the analysis quite more complicate than if a solid spar had been employed for the analysis. Rougher meshes gave trouble because the mesh could not be created around the circular geometry of the spar.

Figure 17: Mesh employed in the structural analysis of the semispar.

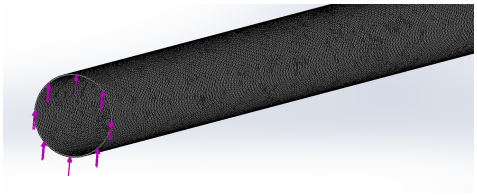

(a) Representation of the mesh.

Malla Detalles

Nombre de estudio	Análisis estático 1 (-Predeterminado-)
Tipo de malla	Malla sólida
Mallador utilizado	Malla basada en curvatura
Puntos jacobianos	4 puntos
Tamaño máx. de elemento	2.29471 mm
Tamaño mín. de elemento	0.1 mm
Calidad de malla	Elementos cuadráticos de alto orden
Número total de nodos	1801010
Número total de elementos	943839
Cociente de aspecto máximo	19.719
Porcentaje de elementos con cociente de aspecto < 3	70.1
Porcentaje de elementos con cociente de aspecto > 10	0.0837
% de elementos distorsionados (Jacobiano)	0
Tiempo para completar la malla (hh:mm:ss)	00:04:24
Nombre de computadora	

(b) Mesh details.

7 Propulsion

In the first Conceptual Design the weight estimation of the propulsive group was done with an approximation of the weight given by Noth [2007]. He gives an overall weight to power ratio of 8kg/kW, which in our case gave a weight of the propulsive plant of $\sim 700g$. We also approximated the total efficiency of the propulsive group $\eta_p \approx 70\%$. Now we'll go one step further and see if this estimations were good enough. The results, in fact, show that both the performance and the weight of the propulsion sysyem are under expected (lower efficiency and higher weight). The final value of efficiency is $\eta_p = 59,8\%$ and the weight is of 888g, 185g over the expected. The propeller is prepared to withstand loads that will never be applied to it, so the author thinks that in future changes it is a priority to lower the weight of the propeller, even if the toughness of the materials is also reduced.

7.1 Propeller

The propeller has been designed and sized with [JavaProp] web applet. JavaProp is a free distributed online-available software that designs a propeller and calculates its basic parameters in a very simple way. It has only a few airfoils to choose and it is not aimed to be a precision tool, but it will be useful for its simplicity and promptness of use at this stage of the design.The results of the design are summarized in table 17.

Number of Blades	2
Revolutions per minute	1000 rpm
Diameter	100 cm
Efficiency	73%
Torque	0,77 N · m
Airfoil	ARA D 6% (Re = 50.000)

Table 17: Main dimensions and characteristics of the propeller design. Obtained with [JavaProp].

This propeller would obviously need to be manufactured specifically for this process as high altitude propellers are not in line production. However, a propeller has been chosen, as if we were to use it, for the sole purpose of defining the weight and the price of a propeller. The chosen model is a PJP-T-L 40x10 specially designed for low kv (high torque) electric motors, made out of carbon fiber and manufactured by Xoar. Its main characteristics can be seen in table 18; note that the diameter is slightly bigger than the design diameter but in the end the hub dimensions reduce the effective area of the propeller and the result can be considered the same. Another thing to be said about this propeller is that it is far too heavy; provided that it also withstands torques much higher than needed (as can be seen in the [Xoar] webpage).

Number of Blades	2
Rpm max.	4000 rpm
Diameter	101,6 cm
Shaft size	10 mm
Weight	380 ± 15 g
Material	CFRP (3k carbon fiber fabric)

Table 18: Specs of Xoar Propeller model PJP-T-L 40x10. Obtained from [Xoar] webpage.

7.2 Motor

The motor chosen is manufactured by Maxon; its identification number is 148867. It has a maximum power of 150W, which means that in cruise conditions the motor would be working at 57,3% throttle. It is thought to be used with a gearhed of (at least) a reduction ratio of 4,5:1. The efficiency, of 91%, is among the best in this size of motors, although we don't know at what point this efficiency is given. The other relevant characteristics of the motor are summarized in table 19.

Weight	480 g
Max. effciency	91 %
Rated Power	150 W
Max. continuous torque	177 mNm
Operating temperature	-30 to 100ºC

Table 19: Specifications of the Maxon RE motor (serial number 148867). From [Maxon] webpage.

7.3 Gearbox

Seeing the characteristics of the propeller, the motor and the gearbox have been chosen at the same time afterwards. The requirements of the motor were relatively high on torque, which meant choosing either a high torque motor with low reduction ratio of the gearbox, or a low to normal torque motor with a high reduction ratio of the gearbox. Whenever possible, the former is always more advisable because the higher the reduction ratio, the lower the efficiency of the power conversion. To give an example, with a reduction ratio of 5:1 the efficiency moves around 90%. Lower efficiencies than that cannot be tolerated.

The products of Maxon, Portescap, Faulhaber and Minimotor (recommended by Noth [2007]) have been examined thoroughly, and some extra search in the internet has been done. However, no proper gearbox has been found to fit the requirements of the project, which means that a custom one should be manufactured. Faulhaber is the manufacturer with more options regarding gearheads, but this producer has not much offer particularly with the desired reduction ratio. The gearhead chosen, whose characteristics can be seen in table 20, has the adequate reduction ratio but does not reach the required torque resistance; however it has been judged that a custom gearbox would be very similar to this one.

Weight	28 g
Max. effciency	90%
Max. input speed	8000 rpm
Operating temperature	-30 to 100ºC
Reduction ratio	4,5:1
Max. continuous torque	550 mN · m
Max. intermitent torque	800mN · m

Table 20: Specifications of the Faulhaber gearbox of the Series 17/1. Obtained from [Faulhaber] webpage.

8 Conclusions

Now it is time to look at the work done, make a little summary of the achievements and of the things left undone, that hopefully someone else will retake at some moment and make the design go further. First of all, say that the main objective has been reached: an UAV able to fly for 24h non-stop has been designed successfully (up to a preliminary design extent). Looking back to the scope of the project, most of the tasks planned have been carried out successfully, they are listed below:

- The solar panels have been sized so that the power plant and the other electric devices have enough power at any time of the day or the night.
- A Flight Control System, able to control the attitude and position of the UAV at any moment, has been chosen, which also integrates a Global Navigation Satellite System.
- A data link device, which allows communication with ground, has been selected.
- The whole propulsive system has been sized, including the motor, the propeller and the gearbox.
- The main aerodynamic surfaces —that is: the wing, the horizontal and the vertical tail— have been sized, along with their position and angle of attack, in a way that ensures weight compensation and longitudinal balance.
- The structure of the plane has been mostly designed and a basic structural analysis of the main spar has been carried out in order to ensure the integrity of the wing.
- A CAD design of the aircraft has been made, along with the drawings that show the location of the main elements of the airframe.
- A budget of the project has been done. It includes both the cost of the design up to this moment and the cost of each element or material of the plane.

However, there have also been some tasks that have not been carried out as expected, be it because of time limitations, or because those tasks finally didn't apply to the current project.

- A slightly deeper study of the electric and electronic system is left to do. Namely, there is an element called Maximum Power Point Tracker that is necessary for every photovoltaic system, and it has not been possible to find one.
- Although the driver motors necessary to move the control surfaces have been taken into consideration, not so the control surfaces themselves.
- Initially it was expected that a fuselage would be needed, but it has been found that considering all the elements that have been part of the design, there was no need of a fuselage, so it has not been designed and it is believed that all the elements can be fit into the wing itself.
- A thorough work has been done concurrently, including an aerodynamic, propulsive and structural study, to achieve longitudinal stability, which one of the most important parameters of a plane. However, the lateral and directional stabilities have not been assessed and are left as task for the future.

8.1 Further Work

Although the work done foresees that an airplane of these characteristics is possible, we should be realistic about the progress of the design. There are still many elements to be sized and validations to be made — above them, the thermal viability, which might well suppose an unconquerable target in a further step of the design. Next are listed and explained the tasks of the following step of the design:

- As just said, a **Thermal Study** of the plane is needed no matter what. The batteries, to give an example, will need dedicated heating almost for sure — if not, at least a system that takes advantage of the heat losses of other elements and a very good insulation of the overall plane. This also applies to most of the other systems; none of them being thought to operate at temperatures below $200K$, so insulation is needed also for the Onboard Systems and the propelling motor.
- Once the dependencies upon parameters are understood and an assessment of the approximations has been made, the Conceptual Design programme can be easily improved, and used to find a configuration more optimal to the problem. The amount of solar cells should be calculated for each combination of parameters AR and S_W; besides, an effort should be made to include the tail sizing in the same programme that makes the optimization.
- Initially, there was the concern that taper ratio or dihedral would someway be detrimental to the design, in the sense that they would limit the number of solar cells placed in the wing. However, it has been seen that —at least in the equator— the solar cells needn't occuy the whole wing, so taper ratio and dihedral can be incorporated without problem.
- A study should be carried out to assess the stability requirements of this kind of aircraft. The stability requirements for commercial aircraft or sailplanes are not applicable, as long as the conditions these aircraft face are completely different.
- The possibility of placing the rotor at the back should be considered. On the one hand, this moves a considerable amount of mass backwards, so the center of gravity is displaced aft, which would mean a bigger tail to maintain the same figures of longitudinal stability. On the other hand, the current design gives some room to downsize the horizontal stabilizer if the motor is placed in the tail, this way contributing to counteract the moments generated by the wing. However, the main reason for it would be that this configuration allows an easy belly landing, whereas a motor placed in the front will always have more probabilities of suffering damage in the landing. If this option is not viable, some other solution should be thought so that the propeller does not hit the ground when landing.
- A CFD study should be considered in a further design come what may. The XLFR5 software gives a good approximation at a low time toll, but it tends to give rather optimistic results. Therefore, a CFD would allow to validate the XFLR5 analysis and also to account for the boom drag, something that has not been possible with XFLR5.
- So far the figures used for efficiency or power consumption have been the normalized ones given by the manufacturers. A further study of the efficiency and power consumption of each element should be done. Besides, the loss of efficiency of the batteries, the solar cells, etc. have to be taken into account also, because those are the parameters that really limit the autonomy of such UAV.

- Something else can be done to improve the autonomy that has not been mentioned yet. Firstly, the **zigzag strategy**: there is an amount of spare energy during the day that is unused and could be employed in gaining altitude; then, during the night (when the energy is more limited), the UAV could glide gently losing the least amount of energy possible. At the end of a 24h period, the plane wouldn't have lost altitude. The second strategy is to train the autopilot to make profit of the thermal updrafts, if they exist in the stratosphere.
- In general, a specific thought should be given to the placing of some elements (like the batteries, or the motor), and the fittings between structural elements like the spars and the boom. Besides, an analysis of the distribution of the batteries and solar cells (among others) along with the wingspan should be done in order to minimize the forces withstood by the spar.

8.2 A Comment of the Author

The aircraft designed in this thesis is considered to be nothing more than a first approach to the design of a HALE UAV. The most valuable outcome of this work has been, therefore, the knowledge gained on the ambit of High Altitude aircraft and on solar powered flights. Some of the most valuable lessons learnt in this project, regarding the design of HALE UAV, are the following:
HALE UAV are the only viable solution to achieve long flights (of the order of months) because it is the only way to ensure a mimimum of daily irradiance. However, there are some difficulties that should be overcame. The lower density of air at their altitudes supposes an increase of the propulsive power necessary. The temperatures are so low (of the order of $\sim 200K$ that thermal insulation might not be enough, and so dedicated heating might be needed by some elements like the batteries or the motor, in order to keep the desired levels of efficiency and to avoid icing. Finally, the lightweight structures of those planes mean that they are weak and really sensitive to turbulence, which in case to be encountered may cause them to crash (like happened to the HELIOS prototype).

References

Airfoil Tools. Airfoil Tools. URL http://airfoiltools.com/.

John D Anderson. *Fundamentals of Aerodynamics, Sixth Edition*. 2017. ISBN 9781259129919.

CFD Online. Sutherland's law – CFD-Wiki, the free CFD reference. URL https://www.cfd-online.com/Wiki/Sutherland's_law.

Tommy Chen and Joseph Katz. Induced Drag of High-Aspect Ratio Wings. In *42nd AIAA Aerospace Sciences Meeting and Exhibit*, Reston, Virigina, jan 2004. American Institute of Aeronautics and Astronautics. ISBN 978-1-62410-078-9. doi: 10.2514/6.2004-38.

Kevin Desmond and Ivo Boscarol. *Electric airplanes and drones : a history*. 2018. ISBN 9781476669618.

Faulhaber. FAULHABER Drive Systems. URL https://www.faulhaber.com/en/products/precision-gearheads/planetary-gearheads/.

Giacomo Frulla. HELIPLAT: Structural Analysis of High Altitude Very Long Endurance Solar Powered platform for telecommunication and Earth Observation Applications. *ICAS Congress*, pages 1–10, 2004.

Bart D. Hibbs, Peter B.S. Lissaman, Walter R. Morgan, and Robert L. Radkey. US Patent 5,810,284, 1998.

Klaus P Hoinka. Temperature, Humidity, and Wind at the Global Tropopause. Technical report, Institut für Physik der Atmosphäre, 1998. URL https://journals.ametsoc.org/doi/pdf/10.1175/1520-0493%281999%29127%3C2248%3ATHAWAT%3E2.0.CO%3B2.

JavaProp. JavaProp - Design and Analysis of Propellers. URL https://www.mh-aerotools.de/airfoils/javaprop.htm.

E. Kaplani, S. Kaplanis, and S. Mondal. A spatiotemporal universal model for the prediction of the global solar radiation based on Fourier series and the site altitude. *Renewable Energy*, 126: 933–942, oct 2018. ISSN 0960-1481. doi: 10.1016/J.RENENE.2018.04.005. URL https://www.sciencedirect.com/science/article/pii/S0960148118304129.

Maxon. maxon motor - Motores DC o Brushless customizados de máxima calid. URL https://www.maxonmotor.es/maxon/view/content/index.

Barnes Warnock McCormick. *Aerodynamics, aeronautics, and flight mechanics*. Wiley, 1995. ISBN 0471110876.

MicroLink. MicroLink Devices, Inc. - Home. URL http://mldevices.com/.

Mitsubishi Polyester Film. HOSTAPHAN® polyester films — Mitsubishi Polyester Film GmbH. URL https://www.m-petfilm.de/en/hostaphan-polyester-films/.

K. Mohanakumar. *Stratosphere Troposphere Interactions*. Springer Netherlands, Dordrecht, 2008. ISBN 978-1-4020-8216-0. doi: 10.1007/978-1-4020-8217-7. URL http://link.springer.com/10.1007/978-1-4020-8217-7.

Leland M. Nicolai and Grant E. Carichner. *Fundamentals of Aircraft and Airship Design*, volume I. American Institute of Aeronautics and Astronautics, Reston ,VA, jan 2010. ISBN 978-1-60086-751-4. doi: 10.2514/4.867538. URL http://arc.aiaa.org/doi/book/10.2514/4.867538.

Andre. Noth. *Design of Solar Powered Airplanes for Continuous Flight*. PhD thesis, 2007.

PVGIS. JRC Photovoltaic Geographical Information System (PVGIS) - European Commission. URL http://re.jrc.ec.europa.eu/pvg_tools/en/tools.html.

ROHACELL. ROHACELL - High-performance structural foam cores. https://www.rohacell.com/product/rohacell/en/. URL https://www.rohacell.com/product/rohacell/en/.

Kenneth Sassen, Zhien Wang, and Dong Liu. Global distribution of cirrus clouds from cloudsat/cloud-aerosol lidar and infrared pathfinder satellite observations (calipso) measurements. *Journal of Geophysical Research: Atmospheres*, 113(D8), 2008. doi: 10.1029/2008JD009972.

Selig, Donovan, and Fraser. Airfoils at Low Speeds. pages 1–408, 1989.

Skybrary. Jet Stream - SKYbrary Aviation Safety. URL https://www.skybrary.aero/index.php/Jet_Stream.

Toray Composites. Toray Composite Materials America, Inc. > Home. URL https://www.toraycma.com/.

UAVN. UAV Navigation — Cutting-edge Autopilots. URL https://www.uavnavigation.com/.

UCAR. UCAR - Center for Science Education. URL https://scied.ucar.edu/.

VOLZ. Standard Servos. URL https://volz-servos.com/produkte/standard/.

Wikipedia. List of Cloud Types, a. URL https://en.wikipedia.org/wiki/List_of_cloud_types.

Wikipedia. HELIOS Prototype, b. URL https://en.wikipedia.org/wiki/Helios_Prototype.

Wikipedia. Airbus Zephyr, c. URL https://en.wikipedia.org/wiki/Airbus_Zephyr.

XFLR5. XFLR5 Guidelines v6.03 - Analysis of foils and wings operating at low Reynolds numbers. Technical report, 2013. URL http://paul.chavent.free.fr/xflr5/Guidelines_v604_en.pdf.

Xoar. Xoar PJP-T-L Quadcopter & Multicopter Propellers made with Carbon Fiber - Precision Pair Propeller For Electric Low Kv Motor. URL https://www.xoarintl.com/multicopter-propellers/precision-pair/PJP-T-L-Precision-Pair-Multicopter-Carbon-Fiber-Propeller-Low-Kv-Motor/.